(2)

FINAL TECHNICAL REPORT

ENERGY PARTITIONING IN HIGH SPEED IMPACT OF ANALOG SOLID ROCKET MOTORS

William P. Schonberg
Civil & Environmental Engineering Department
University of Alabama in Huntsville
Huntsville, Alabama 35899

April 1994

Prepared for:
U.S. Army Space & Strategic Defense Command
Huntsville, Alabama 35807-3801

Contract No. DASG60-89-C-0129-TE-12

Distribution unlimited; approved for public release.

Unclassified
SECURITY CLASSIFICATION OF THIS PAGE

REPORT DOCUMENTATION PAGE

Form Approved OMB No. 0704-0188

1a. REPORT SECURITY CLASSIFICATION Unclassified	1b. RESTRICTIVE MARKINGS
2a. SECURITY CLASSIFICATION AUTHORITY	3. DISTRIBUTION/AVAILABILITY OF REPORT Distribution A: Approved for Public Release; distribution is unlimited.
2b. DECLASSIFICATION/DOWNGRADING SCHEDULE	
4. PERFORMING ORGANIZATION REPORT NUMBER(S)	5. MONITORING ORGANIZATION REPORT NUMBER(S)
6a. NAME OF PERFORMING ORGANIZATION The University of ALabama in Huntsville 6b. OFFICE SYMBOL (If applicable)	7a. NAME OF MONITORING ORGANIZATION USASSDC
6c. ADDRESS (City, State, and ZIP Code) The University of Alabama in Huntsville Civil Engineering Department Huntsville, AL 35899	7b. ADDRESS (City, State, and ZIP Code) P.O. Box 1500 Huntsville, AL 35807 - 3801
8a. NAME OF FUNDING/SPONSORING ORGANIZATION U.S. Army Space & Strategic Defense Command 8b. OFFICE SYMBOL (If applicable) CSSD-TE-T	9. PROCUREMENT INSTRUMENT IDENTIFICATION NUMBER DASG60-89-C-0129 TE-12
8c. ADDRESS (City, State, and ZIP Code) U.S. Army Space & Strategic Defense Command P.O. Box 1500 Huntsville, AL 35807-3801	10. SOURCE OF FUNDING NUMBERS PROGRAM ELEMENT NO. / PROJECT NO. / TASK NO. / WORK UNIT ACCESSION NO.
11. TITLE (Include Security Classification) Energy Partitioning in High Speed Impact of Analog Solid Rocket Motors	
12. PERSONAL AUTHOR(S) Dr. William P. Schonberg	
13a. TYPE OF REPORT Final Technical	13b. TIME COVERED FROM May 1993 TO Dec. 1993
14. DATE OF REPORT (Year, Month, Day) 1994, March	15. PAGE COUNT 58
16. SUPPLEMENTARY NOTATION Available from Defense Technical Information Center (DTIC)	

17. COSATI CODES			18. SUBJECT TERMS (Continue on reverse if necessary and identify by block number)
FIELD	GROUP	SUB-GROUP	Energy Partitioning, Solid Rocket Motors, bullet and fragment impacts, impact loadings, analytical models, ballistic impact hazards, fragmentation, perforation, delamination, propellant simulant, insensitive munitions

19. ABSTRACT (Continue on reverse if necessary and identify by block number)

Modeling the response of solid rocket motors to bullet and fragment impacts is a high priority among the military services from standpoints of both safety and mission effectiveness. Considerable effort is being devoted to characterizing the bullet and fragment vulnerability of solid rocket motors, and to developing solid rocket motor case technologies for preventing or lessening the violent responses of rocket motors to these impact loadings. Because full-scale tests are costly, fast-running analytical methods are required to characterize the response of solid rocket motors to ballistic impact hazards. In this study, a first-principals-based mathematical model is developed to determine the partitioning of the kinetic energy of an impacting projectile among various solid rocket motor failure modes. Failure modes considered in the analyses include case perforation, case delamination, and fragmentation of the propellant simulant material. Energies involved in material fragmentation are calculated using a fragmentation scheme based on a procedure developed in a previous impact study utilizing propellant simulant material. The model is found to be capable of predicting a variety of response characteristics for analog solid rocket motors under high speed projectile impact. Suggestions are made for improving the model and extending its applicabilty to a wider class of impact scenarios.

20. DISTRIBUTION/AVAILABILITY OF ABSTRACT ☒ UNCLASSIFIED/UNLIMITED ☐ SAME AS RPT ☐ DTIC USERS	21. ABSTRACT SECURITY CLASSIFICATION Unclassified
22a. NAME OF RESPONSIBLE INDIVIDUAL Dr. Ben Thomas	22b. TELEPHONE (Include Area Code) (205) 955-4813 / 22c. OFFICE SYMBOL CSSD-TE-T

DD Form 1473, JUN 86 Previous editions are obsolete. SECURITY CLASSIFICATION OF THIS PAGE

This side left intentionally blank.

TABLE OF CONTENTS

This side left intentionally blank.

1.0 INTRODUCTION

The use of insensitive munitions (IM) is a high priority among the military services from standpoints of both safety and mission effectiveness. The response of solid rocket motors to bullet and fragment impacts is an important factor in meeting IM propulsion objectives. Considerable effort is being devoted to characterizing the bullet and fragment vulnerability of solid rocket motors, and to developing solid rocket motor case technologies for preventing or lessening the violent responses of rocket motors to these impact loadings. The principle hazards of concern include prompt shock-initiated detonation, delayed detonation, and violent explosion of motor propellants from bullet and fragment impact. Because full-scale tests are costly, fast-running analytical methods are required to characterize the response of solid rocket motors to ballistic impact hazards [1].

In an attempt to more fully understand the phenomena involved in the response of a solid rocket motor to bullet and fragment impact, a first-principles-based mathematical model was developed to determine the partitioning of the kinetic energy of the impacting projectile among various solid rocket motor failure modes. This kind of information is required in the design of the various components of IM propulsion systems, such as the motor case or the propellant grain. Failure modes considered in the analyses included case perforation, case delamination, and fragmentation of the propellant simulant material. Energies involved in material fragmentation were calculated using a fragmentation scheme based on a procedure developed in a previous impact study utilizing propellant simulant materials [2-4]. These quantities were computed for the fragmentations caused by the initial projectile impact and for those caused by the impact of the residual projectile on the rocket motor rear wall.

Figure 1 shows a sketch of a generic rocket motor that is impacted by a cylindrical projectile. In this study, we consider two impact scenarios. In the first, the impact velocity is sufficiently high so that the projectile perforates the near case and propellant simulant layers, but not high enough so that it can perforate the far case and simulant material layers. In the second,

the impact velocity is high enough so that the projectile is able to perforate both sides of the rocket motor and exit with some residual kinetic energy. In this manner, the model developed herein can serve as the basis for a more detailed phenomenological model that considers a much broader range of impact conditions. However, the development of such a model must include an experimental component whereby empirical evidence is obtained to guide its development.

2.0 SOLID ROCKET MOTOR IMPACT PHENOMENA

Consider the impact of a high speed projectile on a generic solid rocket motor. The trajectory of the projectile is such that the projectile's longitudinal axis is perpendicular to that of the analog motor (i.e. no obliquity and no yaw). The analog motor consists of a layer of propellant simulant material bonded to a filament wound case. The portion of the filament wound case and the propellant simulant material to first experience the effects of the impact are referred to as the 'near' case and simulant material layers; corresponding layers to feel the effects of the impact subsequent to the perforation of the near layers are referred to as 'far' material layers. The following discussion of the phenomena involved in the perforation and fragmentation of solid rocket motors is an adaptation of the discussion presented in Ref. [5].

Upon impact, strong inelastic waves propagate through the case material. These waves propagate radially outward from the impact site and transversely through the thickness of the solid rocket motor wall. The radial waves damage the case material surrounding the impact site. This damage can appear as delaminations, fiber pull-out, fiber/matrix fracture, etc. At the case/simulant interface, a portion of the energy associated with the transverse propagation of the waves created by the impact is reflected back into the case material in the form of release waves while the remainder of the energy is transmitted into the simulant material in the form of compression waves. These waves travel through the propellant simulant material and eventually reflect from the free surface as tensile waves. The backward propagation of these tensile waves and their interaction with forward propagating compression waves causes some fracture of the rear surface of the simulant material to occur.

Simultaneous to the motion of the impact-induced waves in the case and simulant materials, the projectile travels through the case and simulant materials creating a tunnel in the simulant material. Its velocity naturally decreases as some of its energy has been absorbed by the perforation of the near case layer. The propellant simulant material ahead of the projectile begins to disintegrate when it experiences stresses that are either in excess of its ultimate tensile strength or its dynamic fracture toughness. This creates a cloud of propellant simulant debris that travels

across the bore and impacts the far layer of propellant simulant material. If sufficient kinetic energy is available, the projectile also impacts the far propellant simulant layer.

The impact of the debris cloud on the far propellant simulant material layer will naturally damage the simulant material. If the kinetic energy of the original projectile is sufficiently high, then it is entirely likely that the projectile will perforate the far simulant layer. The mode of far simulant material perforation is very much the same as that of the near simulant material layer. The projectile tunnels through the simulant material, eventually disintegrating the plug of material that forms ahead of it. Finally, if sufficient kinetic energy remains, the projectile may perforate the far case layer and exit the rocket motor with some residual kinetic energy.

Based on this discussion, the following energy balance exists for the initial impact:

Initial Projectile Kinetic Energy = Energy Required to Perforate the Near Case Layer
+ Energy Absorbed by Damage to Case Material Surrounding the Impact Site
+ Energy Required to Fragment the Near Propellant Simulant Material Layer
+ Energy Required for Simulant Debris Motion
+ Initial Projectile Residual Kinetic Energy (if any) (1)

If there is non-zero initial residual projectile kinetic energy, then it is absorbed by the various phenomena associated with the impact and possible perforation of the far material layers. Thus, the following energy balance can be written for the final residual projectile kinetic energy:

Final Projectile Residual Kinetic Energy = Initial Projectile Residual Kinetic Energy
- Energy Required to Fragment the Far Propellant Simulant Material Layer
- Energy Absorbed by Damage to Case Material Surrounding the Far Impact Site
- Energy Required to Perforate the Far Graphite/Epoxy Case
- Energy Required for Exterior Simulant Debris Motion After Case Perforation (2)

The focus of the remainder of this paper will be to develop mathematical expressions for each of the terms in equations (1) and (2). However, the complexity of the problem dictates that certain assumptions and simplifications are required to bring the problem down to solvable proportions. These assumptions and simplifications are discussed in the next section.

3.0 MODEL ASSUMPTIONS AND SIMPLIFICATIONS

In developing the first-principles-based model of kinetic energy partitioning for the impact of an analog solid rocket motor, a number of simplifying assumptions were employed. These assumptions are discussed in the following paragraphs.

First, the projectile is assumed to be made of a hardened metallic material such as steel with a cylindrical shape and a blunt nose. The filament wound case is presumed to consist of graphite fibers wound using an epoxy as the matrix material; the propellant simulant material is presumed to be essentially rubber. Further comments regarding material properties will be made in Chapter 6.

Second, the cylindrical analog motor is modeled as two parallel flat plates (see Figure 2). While such a simplification can be expected to have some influence on the perforation and fragmentation response characteristics, the deviations of the flat plate characteristics from those in which a cylindrical geometry were used are expected to be minimal (see, e.g. [6]). As such, it would not be unreasonable to neglect them in the development of a first-principles based model of impact response.

Third, the projectile is assumed to remain undeformed as it perforates the near filament wound case wall, the near propellant simulant layer, and, in the event that it exits the analog motor, the far propellant simulant material and the far filament wound case wall. This is a reasonable assumption given the fact that the impacting fragment is presumed to be made of a high-strength hardened metallic material such as steel, whereas the filament wound case and the propellant simulant material are made from materials of comparable or lower strength.

Fourth, the hole in the near, and if appropriate far, case wall is assumed to have a diameter equal to that of the impacting fragment. This is also a reasonable assumption given the relative strengths of the materials involved. In addition, if the impact velocities considered sufficiently exceed the ballistic limit of the case material, but not to the point where the materials significantly melt or burn, then the holes created in the case walls would also not be expected to significantly exceed that of the impacting projectile.

Fifth, the cavity in the propellant simulant material is also presumed to be approximated by the shape shown in Figure 3. This shape is based on photographs obtained from experimental studies in which blunt nosed projectiles impacted slabs of propellant simulant material. The relationships between h, h_1, and θ_c as shown in Figure 3 will be discussed in the next section. As a direct corollary of the second assumption, it is also presumed that the diameter of the initial cylindrical portion of the cavity shown in Figure 3 has a diameter also equal to that of the impacting projectile.

Sixth, energy absorbed by the elastic response of the case walls following the impact and that lost due to viscous heat dissipation is presumed to be negligible and ignored. The justification for the neglect of energy consumption by elastic deformation and heat dissipation lies in the fact that the impact event is presumed to be rapid when compared with the strain rates associated with elastic response and with heat dissipation.

Finally, the fragmented far simulant material is presumed to remain within the rocket motor, and in the event of far case wall perforation, only the projectile is ejected from the motor. This appears to be a reasonable assumption because the far graphite/epoxy layer confines the simulant material and generally prevents its motion.

4.0 FRAGMENTATION OF PROPELLANT SIMULANT MATERIAL

As part of the development of the energy partition model, a model of the fragmentation of the propellant simulant material must be developed. While numerous fragmentation schemes currently exist, they have been developed primarily to model the processes involved in the fragmentation of either ductile or brittle solid materials such as metals and rocks. Thus, the fragmentation model for the propellant simulant material to be developed here is semi-analytical, that is, it is based on empirical evidence but presented as a closed-form analytical expression.

Based on the results of a curve-fitting exercise performed using the data provided in a recent study of the fragmentation of propellant simulant materials [2-4], we postulate that the number of simulant fragments $N_f(r)$ with a radius less than or equal to a specified value r is given as follows:

$$N_f(r) = Ar^{-2} \tag{3}$$

where A is a constant that needs to be determined and r is the characteristic radius of a propellant fragment.

To determine the constant A, we equate the total mass of propellant simulant that is fragmented to the total mass of fragments whose size distribution is governed by equation (3). Since the volume of propellant simulant fragments is equal to the volume of the cavity created in the simulant material, and since the cavity may be said to consist of a cylinder resting on a cone, we have the following equality for fragmented simulant mass:

$$\pi R_c^2 (h - h_1)/3 + \pi R_p^2 h_1 = -\int_{a_{min}}^{a_{max}} m(r)\,dN_f(r) = -\int_{a_{min}}^{a_{max}} m(r)\frac{dN_f}{dr}dr \tag{4}$$

where h is the thickness of the simulant material layer, h_1 is the depth of the cylindrical portion of the cavity, R_p is the radius of the projectile, and R_c is the radius of the base of the conical portion of the cavity. The quantities a_{max} and a_{min} refer to the radii of the largest and smallest simulant material fragment; $m(r)=4\pi r^3\rho_{ps}/3$ is the mass of a fragment with radius r and mass density ρ_{ps}. Substituting equation (3) into equation (4), performing the integration, and solving for A yields

$$A = \left(\frac{3}{8}\right)\left[\frac{R_c^2(h-h_1)/3 + R_p^2 h}{a_{max} - a_{min}}\right] \tag{5}$$

where the quantities R_c, h_1, a_{max}, and a_{min} are still to be determined.

From Figure 3, R_c is simply given by

$$R_c \approx (h - h_1)\tan\theta_c \tag{6}$$

where θ_c is the vertex angle of the conical portion of the simulant material cavity. While the value of θ_c is undoubtedly a function of impact velocity, geometry, and material properties, a reasonable approximation for θ_c is 45 deg [2-4].

The functional form of the quantity h_1 is also based on the empirical evidence provided in Ref. [2-4]. This evidence shows that $h_1 \sim 0$ for impact velocities greatly in excess of the ballistic limit of the simulant material layer and that $h_1 \approx h$ for impact velocities near the ballistic limit. In other words, as the impact velocity is increased beyond the ballistic limit of the propellant simulant material layer, the depth of the leading cylindrical portion of the material cavity decreases from a value that is slightly less than the full thickness of the layer to a value that is near zero. While there are any number of functional forms that meet these criteria, the form chosen for use in this study is given by

$$h_1 / h = e^{\alpha(1 - V_0/U_{BL})} \tag{7}$$

where α is a user-controlled parameter that dictates the actual shape of the function, V_0 is an impact velocity, and U_{BL} is the ballistic limit velocity of the simulant material layer. The actual definition of V_0 and the means of calculating the ballistic limit velocity of the propellant simulant material layer U_{BL} are presented in the next section.

While there is clearly no theoretical limit for the size of a smallest fragment created during the fragmentation process (after all, who is to say that molecular-sized particles were not created?), common sense dictates that a reasonable cut-off value should be chosen. For the purposes of this investigation, a_{min} was arbitrarily set equal to 0.1 mm.

The quantity a_{max} can be obtained by assuming that there is only one particle that has a radius equal to a_{max}. Then, by the definition of N_f, we have

$$N_f(r = a_{max}) = 1 \tag{8}$$

Substituting for N_f according to equation (3) yields

$$\frac{A}{a_{max}^2} = 1 \tag{9}$$

so that

$$a_{max} = \sqrt{A} \tag{10}$$

Substituting for A according to equation (5) and rearranging yields

$$a_{max}^2(a_{max} - a_{min}) - \eta = 0 \tag{11}$$

where

$$\eta = \left(\frac{3}{8}\right)\left[R_c^2(h - h_1)/3 + R_p^2 h_1\right] \tag{12}$$

Equation (11) is a cubic equation for a_{max}. To solve it, we first rewrite it in the following more standard for:

$$y^3 + py^2 + q = 0 \tag{13}$$

where $y=a_{max}$, $p=-a_{min}$, and $q=-\eta$. Following the standard procedure for the solution of a third degree polynomial, we first strive to eliminate the y^2 term. This is accomplished with the substitution

$$y = x - \frac{p}{3} \tag{14}$$

in equation (13). The equation obtained is then written as follows:

$$x^3 + 3Hx + G = 0 \tag{15}$$

$$H = -\frac{p^2}{9} = -\frac{a_{min}^2}{9} \tag{16a}$$

$$G = \frac{2p^3 + 27q}{27} = -\frac{2a_{min}^3}{27} - \left(\frac{3}{8}\right)\left[R_c^2(h - h_1)/3 + R_p^2 h_1\right] \tag{16b}$$

According to Cardan's Formula [7], a solution to equation (15) is given by

$$x = \left(\frac{-G+\sqrt{G^2+4H^3}}{2}\right)^{1/3} + \left(\frac{-G-\sqrt{G^2+4H^3}}{2}\right)^{1/3} \tag{17}$$

Since equation (15) has three roots, it is also desirous to determine the remaining two roots. However, by invoking some basic principles from the theory of equations, we can infer some information regarding the nature of the remaining two roots without having to solve for them.

Consider the quantity

$$D = -27(G^2+4H^3) \tag{18}$$

If $D<0$, equation (15) has 1 real and 2 imaginary roots; if $D=0$, equation (15) has 3 equal real roots; and, if $D>0$, then equation (15) has 3 distinct real roots. Substituting for G and H according to equations (16a,b) into equation (18) and simplifying results in the following expression for D:

$$D = -27\left(\frac{4a_{min}^3\eta}{27} + \eta^2\right) \tag{19}$$

Since $a_{min}>0$ and $\eta>0$, it follows that $D<0$ and equation (15) has only one real root. Hence, the other two roots of equation (15) are imaginary and can be ignored. The question then remains as to whether the root given by equation (15) is in fact the real root or one the imaginary roots. Since the discriminant in each of the terms in equation (15) is simply -D/27 and since $D<0$, the discriminant will be a positive number so that a non-imaginary square root will be obtained. Hence, the root given in equation (15) is in fact the sole real root of equation (15). The value of x obtained using equation (15) can then be used to define a_{max} by writing equation (14) as follows:

$$a_{max} = \left(\frac{-G+\sqrt{G^2+4H^3}}{2}\right)^{1/3} + \left(\frac{-G-\sqrt{G^2+4H^3}}{2}\right)^{1/3} - \frac{a_{min}}{3} \tag{20}$$

This completes the development of the fragmentation scheme used in this study. The next section addresses the partitioning of the initial kinetic energy of the impacting projectile.

5.0 IMPACT ENERGY PARTITIONING

In this section, the method of partitioning the kinetic energy of the impacting projectiles is discussed. The overall approach behind the method is to base the analytical formulation on the symbolic equations (1) and (2) and, in doing so, incorporate some of the simplifying assumptions discussed previously. Thus, we first consider equation (1) and the initial impact on the near case and simulant material layers, and follow with a consideration of the far simulant material and case layers.

5.1 Impact of Near Case and Simulant Material Layer

In this part of the development, we assume that the residual kinetic energy of the projectile after passing through the near case and simulant material layers is not sufficient for perforating the far simulant material and case layers. Taking into account the simplifications and assumptions already discussed, equation (1) can then be written as

$$E_{proj}^{init} = E_{perf}^{gr/ep} + E_{delam}^{gr/ep} + E_{frag}^{ps,cr} + E_{frag}^{ps,mv} + E_{proj}^{resid} \tag{21}$$

where E_{proj}^{init} is the initial kinetic energy of the impacting projectile. The five energies on the right hand side of equation (21) correspond to the energies required to perforate the near case layer, to delaminate the case, to fragment the propellant simulant material, to move the debris cloud consisting of simulant material fragments across the bore, and the residual kinetic energy of the projectile, respectively.

The first two terms on the right hand side of equation (21) are simply written as

$$E_{init} = \frac{1}{2} m_p V_p^2 \tag{22a}$$

$$E_{perf}^{gr/ep} = \frac{1}{2} m_p V_{BL}^2 \tag{22b}$$

where $m_p = \pi R_p^2 L_p \rho_{pr}$ is the mass of the impacting projectile, V_{BL} is the ballistic limit of the near graphite/epoxy case layer, and ρ_{pr} is the mass density of the impacting projectile.

To determine the ballistic limit of the near case layer, we assume that the propellant simulant material adjacent to the near graphite/epoxy layer does not significantly affect the value of the ballistic limit. This appears to be a reasonable assumption in view of the fact that the strength of the propellant simulant material is significantly less than that of the case material. In deriving an expression for V_{BL}, we adopt the penetration model developed by Awerbach [8]. Although this model was originally developed for metal targets, it has been shown to yield acceptable results when applied to composite targets as well [9]. In this model, the exit velocity of a projectile perforating a flat target plate is given by

$$V_f = \left[\left(V_i^2 + \frac{\sigma_{ult}}{3\rho/2} \right) \left(\frac{m_o/\rho A}{h + m_o/\rho A} \right)^3 - \frac{\sigma_{ult}}{3\rho/2} \right]^{1/2} \tag{23}$$

where V_i is the impact velocity, A is the hole diameter in the target plate, m_o is the mass of the impacting projectile, and h is the thickness of the target plate; ρ and σ_{ult} are the density of the target plate and ultimate strength of the target plate material. In the event that V_i is the ballistic limit velocity of the target plate, then V_f=0. This condition can be used to solve for V_{BL} of the graphite/epoxy layer:

$$V_{BL} = \left[\left(\frac{\sigma_{ult,gr/ep}}{3\rho_{gr/ep}/2} \right) \left(\frac{m_p/\rho_{gr/ep}A}{h_{gr/ep} + m_p/\rho_{gr/ep}A} \right)^{-3} - 1 \right]^{1/2} \tag{24}$$

where $h_{gr/ep}$ is the thickness of the graphite/epoxy case. Following a similar line of reasoning, we can write the following expression for the ballistic limit of the propellant simulant material:

$$U_{BL} = \left[\left(\frac{\sigma_{ult,ps}}{3\rho_{ps}/2} \right) \left(\frac{m_p/\rho_{ps}A}{h + m_p/\rho_{ps}A} \right)^{-3} - 1 \right]^{1/2} \tag{25}$$

where h is the thickness of the propellant simulant material. Thus, the energy required to perforate the near graphite/epoxy layer is now completely defined.

The energy absorbed by the delamination of the case material is a bit more difficult to define. To calculate absorbed energy, we must first be able to calculate the actual area of delamination that occurs in the case material as a function of velocity, material properties, geometry, etc. To do this without the aid of empirical data is, indeed, quite a challenge. However, not to be deterred from our ultimate goal, we proceed to develop a means for approximating the amount of delamination that occurs that should be suitable for a first-principles based analytical model.

Our method for approximating the amount of delamination is based on a trend observed in previous experimental studies of delamination of composite materials under impact loadings and a little bit of common sense. It has been previously observed that as impact velocity is increased, the total delaminated area in a composite material increases linearly with respect to the kinetic energy of impact, or with respect to the square of the impact velocity [10]. In addition, we expect that as the impact velocity greatly exceeds the ballistic limit of the target plate, the area of delamination will approach a constant value (and may in fact begin to decrease as the impact velocity is increased still more). Thus, the total area of delamination can be approximated as

$$A_{delam} = A_0 f(V_p) \tag{26}$$

where $f(V_p)$ is a function with the anticipated behavior; A_0 is a constant denoting the asymptotic limit of the function defining A_{delam}. An elementary function that exhibits the desired behavior is

$$f(V_p) = 1 - e^{-\beta V_p / V_{BL}} \tag{27}$$

where β is again a user-controlled parameter that defines the shape of the function. Naturally, a question remains as to the value of A_0, the maximum delaminated area. Experimental studies have shown this to be a number on the order of 9 to 10 times the projected area of the impacting projectile (see, e.g. [11]); hence, for this particular investigation, we can write

$$A_{delam} = 9A_p\left(1 - e^{-\beta V_p / V_{BL}}\right) \tag{28}$$

However, we still need to relate A_{delam} to $E_{delam}^{gr/ep}$. This is accomplished as follows.

Suppose the near and far case layers each have N_L layers. If we associate a critical surface energy density γ_c that is required for the formation of a delaminated surface and assume that the area of delamination is constant throughout the thickness of the case, then we can write the total energy required for the delamination of the near case layer as

$$E_{delam}^{gr/ep} = 2(N_L - 1)A_{delam}\gamma_c \tag{29}$$

The '2' on the right hand side of equation (29) arises from the fact that there are two surfaces created in a delamination event. Using the relationship between surface energy density and stress intensity factor, we can write

$$\gamma_c = \frac{K_{IIc}^2}{2\rho c_o^2} \tag{30}$$

where c_o is the speed of sound in the material experiencing fracture (or, as in this case, delamination) and K_{IIc} is the critical mode II stress intensity factor. Naturally, there are various ways of defining sound speed for a composite material, depending on the direction chosen, etc. Since this is a first-principles based model, it will be assumed that the sound speed can be written as

$$c_o = \sqrt{E_{11}/\rho_{ge}} \tag{31}$$

where ρ_{ge} is the density of the graphite/epoxy case material and E_{11} is the modulus in the fiber direction. Using the relationship between stress intensity factor and energy release rate, the following expression is written for the mode II stress intensity factor:

$$K_{IIc} = \sqrt{E_{11}G_{IIc}} \tag{32}$$

where G_{IIc} is the critical energy release rate for inter-layer delamination.

Thus, substituting equations (28,30,31) into equation (29) results in the following expression for the amount of energy absorbed in the delamination of the composite case material:

$$E_{delam}^{gr/ep} = 9(N_L - 1)A_p\left(1 - e^{-\beta V_p / V_{BL}}\right)G_{IIc} \tag{33}$$

To derive an expression for $E_{frag}^{ps,cr}$, the energy required to fragment the propellant simulant material, we follow the procedure developed in Ref. [3] with some slight modifications. Thus, we begin by writing

$$E_{frag}^{ps,cr} = -\int_{a_{min}}^{a_{max}} E_s(r)\frac{dN_f}{dr}dr + A_c\gamma \tag{34}$$

where $E_S(r)$ is the total energy consumption associated with the formation of a single propellant simulant material fragment with radius r, A_C is the surface area of the simulant material cavity, and γ is the surface energy density of the simulant material. In Ref. [3] it is shown that E_S consists of two parts: the strain energy associated with the deformation of a potential fragment until the point of rupture and the surface energy associated with the creation of the fragment surface. Using this formulation, the following expression for $E_S(r)$ is obtained:

$$E_s(r) = \frac{20}{3}\pi\gamma r^2 \tag{35}$$

where γ, as used in equations (34) and (35), is written as

$$\gamma = \frac{K_{ID}^2}{2\rho_{ps}c_{s,ps}^2} \tag{36}$$

where K_{ID}, ρ_{ps}, and $c_{s,ps}=\sqrt{(K_{ps}/\rho_{ps})}$ are the mode I dynamic fracture toughness, density, and sound speed of the propellant simulant material; K_{ps} is the bulk modulus of the propellant simulant material. Substituting for $N_f(r)$ according to equations (3) and (5) and performing the required manipulations results in the following expression for $E_{frag}^{ps,cr}$:

$$E_{frag}^{ps,cr} = \left(\frac{K_{ID,ps}^2}{2\rho_{ps}c_{s,ps}^2}\right)\left\{5\pi\left[\frac{R_c^2(h-h_1)/3+R_p^2}{a_{max}-a_{min}}\right]\ln\left(\frac{a_{max}}{a_{min}}\right)+\pi R_c\sqrt{R_c^2+(h-h_1)^2}\right\} \tag{37}$$

Since the fragmentation of the propellant simulant material is due to the impact of the projectile after it perforates the graphite/epoxy case, the 'impact velocity' used in equation (37) to calculate h_1 is V_f, the reduced velocity of the projectile as defined by equation (23).

This completes the derivation of the expression for the energy absorbed in the fragmentation of the propellant simulant material. The final expression to be derived is that for the kinetic energy of the moving debris cloud. This energy expression is written as follows:

$$E_{frag}^{ps,mv} = \frac{1}{2} m_{dc} V_{dc}^2 \tag{38}$$

where m_{dc} is the total mass of the propellant simulant fragments in the debris cloud and V_{dc} is the velocity of the debris cloud center of mass. Based on the development thus far, the mass of the debris cloud material can be written simply as

$$m_{dc} = \rho_{ps}\pi R_c^2 (h - h_1)/3 + \rho_{ps} R_p^2 h_1 \tag{39}$$

The velocity of the debris cloud is also obtained by following the procedure in Ref. [3]. First, we consider the following energy balance:

$$E_{proj}^{init} - (E_{perf}^{gr/ep} + E_{delam}^{gr/ep}) = E_{avail} + E_{proj}^{resid} \tag{40}$$

where E_{avail} is the amount of energy delivered to the fragmentation volume, i.e. it is the amount of energy available for fragmenting the propellant simulant material and its motion:

$$E_{avail} = E_{frag}^{ps,cr} + E_{frag}^{ps,mv} \tag{41}$$

Thus, if we can derive an independent expression for E_{avail}, we can directly solve for V_{dc} by rewriting equation (41) as follows:

$$\frac{1}{2} m_{dc} V_{dc}^2 = E_{avail} - E_{frag}^{ps,cr} \tag{42}$$

where $E_{frag}^{ps,cr}$ is given by equation (37). Following the procedure in Ref. [3], we write

$$E_{avail} \approx \frac{1}{2} m_{ps}^{cp} (2 V_{ps}^{imp})^2 \tag{43}$$

where m_{ps}^{cp} is the mass of the compressed part of the propellant simulant material and V_{ps}^{imp} is the velocity imparted to the propellant simulant material, that is, it is the particle velocity in the simulant material induced by the passage of the initial shock wave through the material. The presence of the '2' in front of the velocity term in equation (43) is due to the fact that as the shock wave in the propellant simulant material travels through the material and reflects from the rear free surface, it induces motion in the simulant material that is characterized by a velocity equal to twice the particle velocity in the material.

Using the three shock jump conditions to characterize the impact of the projectile on the propellant simulant material after perforation of the graphite/epoxy case and continuity of pressure and material at the impact interface, we obtain the following expression for particle velocity in the propellant simulant material:

$$V_{ps}^{imp} = \frac{b - \sqrt{b^2 - 4ac}}{2a} \tag{44}$$

where

$$a = k_{pr} - k_{ps}\left(\frac{\rho_{ps}}{\rho_{pr}}\right) \tag{45a}$$

$$b = 2k_{pr}V_f + c_{s,pr} + c_{s,ps}\left(\frac{\rho_{ps}}{\rho_{pr}}\right) \tag{45b}$$

$$c = c_{s,pr}V_f + k_{pr}V_f^2 \tag{45c}$$

where the k constants are the slopes of the linear shock wave speed-particle velocity re.ationships for the projectile and propellant simulant materials and the $c_s = \sqrt{K/\rho}$ are the adiabatic sound speeds of the materials.

The mass of the compressed portion of the propellant simulant material can be approximated as the mass of the material directly beneath the projectile as it penetrates into the simulant material, that is,

$$m_{ps}^{cp} = \varepsilon \pi R_p^2 h \rho_{ps} \tag{46}$$

where ε is another user-controlled parameter. Substituting equations (43,44,46) into equation (42) yields the following expression for V_{dc}:

$$V_{dc} = \left[\frac{\frac{\varepsilon}{2} \pi R_p^2 h \rho_{ps} \left(2 V_{ps}^{imp}\right)^2 - E_{frag}^{ps,cr}}{m_{dc}/2} \right]^{1/2} \tag{47}$$

Finally, the expression for the residual velocity of the projectile is written as

$$V_{res} = \sqrt{\frac{E_{proj}^{resid}}{m_p/2}} \tag{48}$$

where E_{proj}^{resid} is the energy remaining after the initial impact energy has been partitioned among the energy absorbing processes discussed, that is,

$$E_{proj}^{resid} = E_{proj}^{init} - (E_{perf}^{gr/ep} + E_{delam}^{gr/ep} + E_{frag}^{ps,cr} + E_{frag}^{ps,mv}) \tag{49}$$

5.2 Impact of Far Case and Simulant Material Layer

If the impact velocity is significantly larger than the ballistic limit of the graphite/epoxy case, then the possibility exists that the projectile will exit the rear of the solid rocket motor. In this case, equation (2) can be rewritten as

$$E_{proj}^{resid} = E_{frag}^{ps,cr} + E_{delam}^{gr/ep} + E_{perf}^{gr/ep} + E_{proj}^{final} \tag{50}$$

In writing equation (50), it is noted that there is no energy allocated to the motion of the propellant simulant fragments created by the far impact. This is due to the presence of the far case layer which prevents the motion of the far simulant material fragments. The quantities E_{proj}^{resid}, $E_{perf}^{gr/ep}$, and $E_{frag}^{ps,cr}$ are defined by equations (49), (22b), and (37), respectively. However,

it is noted that in evaluating $E_{frag}^{ps,cr}$ for the far layer using equation (37), the quantity h_1 is evaluated using an 'impact' velocity of V_{res}, which is the residual velocity of the projectile after exiting the near case and propellant simulant material layers.

The next energy absorbing mechanism considered is the delamination of the far graphite/epoxy case material. Following the procedure used previously, we arrive at the expression

$$E_{delam}^{gr/ep} = 9(N_L - 1)A_p(1 - e^{-\beta V'/V_{BL}})G_{IIc} \tag{51}$$

where V' has been written instead of V_p to take into account the reduced velocity of the projectile. This reduction in velocity is due to the energy loss in fragmenting the far simulant material layer and is obtained from the following energy balance:

$$\frac{1}{2}m_p(V')^2 = E_{proj}^{resid} - E_{frag}^{ps,cr} \tag{52}$$

Substituting for E_{proj}^{resid} according to equation (48) and solving for V' yields

$$V' = \sqrt{V_{res}^2 - \frac{E_{frag}^{ps,cr}}{m_p/2}} \tag{53}$$

where $E_{frag}^{ps,cr}$ is given by equation (37) with h_1 again being evaluated using an 'impact' velocity of V_{res}. Following the calculation of V', it is worthwhile to check and see if $V' > V_{BL}$. If not, there is not enough energy remaining to perforate the far case layer and the projectile becomes embedded in the far propellant simulant layer. If in fact it is true that $V' > V_{BL}$, then it is indeed likely that the projectile will perforate the far case layer and exit the solid rocket motor.

The final kinetic energy of the projectile as it exits the solid rocket motor and its final exit velocity are then readily obtained using

$$E_{proj}^{final} = E_{proj}^{resid} - (E_{frag}^{ps,cr} + E_{delam}^{gr/ep} + E_{perf}^{gr/ep}) \tag{54}$$

and

$$V_{fin} = \sqrt{\frac{E_{proj}^{final}}{m_{pr}/2}} \tag{55}$$

respectively. This completes the analytical development of the energy partitioning model. The next section presents some numerical results using the equations derived herein.

6.0 NUMERICAL RESULTS AND DISCUSSION

A FORTRAN program was written to implement the equations developed in the previous section; its listing is provided in Appendix A. Typical output files are provided in Appendix B. In the implementation of the energy partition model developed herein, the following values were used for the user-controlled constants α,β, and ε:

$$\alpha = 0.25, \qquad \beta = 1.0, \qquad \varepsilon = 0.5 \tag{56}$$

Naturally, experimental information is required to ultimately justify these choices or dictate the use of other values. These specific values were chosen because their use allowed the predictions of the model to be consistent with expected trends in the output as well as with the laws of physics. For example, the specified choice of ε ensured that the velocity of the projectile decreased monotonically as the projectile moves through the rocket motor. An improper choice of ε could actually result in an increase in the projectile velocity after perforating the near case layer and fragmenting the near propellant simulant material. In addition, these choices resulted in ballistic limit values for the graphite/epoxy and the propellant simulant that are consistent with those found in the literature. Specifically, the model developed herein predicted that $V_{BL} \approx 250$ m/sec and $U_{BL} \approx 50$ m/sec. These values are consistent with those cited in Ref.s [9] and [2-4], respectively.

The material properties used in the numerical simulations are given in Table 1. The material properties were obtained by considering the fiber material to be IM6 graphite while the matrix material was taken to be 3501-6 epoxy. The material property values presented in this Table are representative values obtained by averaging several values obtained during a literature survey (see, e.g., [2-4,12-27]). The properties in the column next to the propellant simulant material represent typical thermodynamic and mechanical properties of actual propellant materials. Worthy of note in Table 1 is the fact that, for the most part, the material property values of the propellant simulant material closely resemble those of an actual generic propellant material.

Table 1. Material Properties

Property	Units	Graphite/ Epoxy	Propellant Simulant	Generic Propellant
c_s	km/sec	3.58	2.21	2.18
k	---	0.91	1.87	2.11
Γ_o	---	0.50	1.44	1.15
ρ	gm/cm^3	1.53	1.78	1.73
E	GPa	177.5	2.40	4.98
ν	---	0.39	0.45	0.40
K	GPa	N/A	8.17	8.31
G	GPa	4.62	0.81	1.78
K_{ID}	$MPa\sqrt{m}$	N/A	N/A	1.28
G_{IIc}	J/m^2	400	N/A	N/A
σ_y	MPa	N/A	0.37	N/A
σ_{ult}	MPa	1.38	0.59	N/A

Figure 4 shows plots of the propellant simulant debris cloud velocity and the final projectile velocity as functions of the initial impact velocity. The relationship between the debris cloud velocity and the impact velocity is seen to be relatively constant until the impact speed at which the projectile is able to perforate the far case layer as well (approximately 420 m/sec) and then becomes nearly linear. The plot of the final projectile velocity is also seen to change near an impact speed of 420 m/sec. However, the change in the plot of the final projectile velocity is more dramatic: there is a pronounced 'dip' in the curve. This odd behavior can be explained by the following considerations.

Until the projectile perforates the far case layer, its residual velocity steadily increases from its near zero value when the projectile just barely perforates the near case layer. In this initial regime, the projectile's residual velocity is below the ballistic limit of the case material. As such, the projectile remains embedded in the far simulant layer without perforating the far case

layer. Naturally, as the impact velocity is increased, the depth of embeddment also increases. Finally, when the impact velocity is high enough so that the residual velocity exceeds the far case material's ballistic limit, the projectile perforates the far case layer. However, in doing so a substantial amount of energy is absorbed by the perforation process. Hence, at impact velocities just above those required for far case layer perforation the final projectile velocity will in fact be relatively low. As the impact velocity continues to increase so does the final projectile velocity.

The decrease in the projectile velocity as it moves through the rocket motor is shown in Figure 5. In those cases where far case layer perforation does not occur, it appears that the largest velocity drop is due to the energy expended in perforating the near case layer. However, in those cases where far case layer perforation does occur, the major contributor to the decrease in the projectile velocity is the fragmentation and motion of the near simulant material. Apparently, for relatively low velocity impacts, most of the impact energy is absorbed by the perforation of the near case layer. However, at high impact velocities the creation and propagation of the near propellant simulant material absorbs a significantly larger portion of the initial kinetic energy than does the perforation of the near case layer. Hence, at impact speeds above approximately 1000 m/sec the largest drop in projectile velocity occurs after debris cloud formation. It is interesting to note that the fragmentation of the far propellant simulant material does not result in a similar velocity drop. This fact indicates that it is actually the motion of the debris cloud, rather than its formation, that is absorbing the majority of the kinetic energy and causing the drop in the projectile velocity.

Figure 6 shows the partitioning of the initial kinetic energy among the various response modes considered in this study. Of immediate note is the fact that the energies associated with the delamination of the near and far case layers and the fragmentation of the near and far propellant simulant material layers are not shown. The simple explanation for this is that these response modes typically absorbed less than 0.5% of the initial kinetic energy of the impacting projectile. Hence, their effects on the motion of the projectile were minimal compared with the modes shown. As expected, Figure 6 shows that as the initial impact velocity of the projectile is

increased beyond the point where both near and far material layers are perforated, the bulk of the kinetic energy remains with the projectile as it exits the far wall of the rocket motor.

One area of concern is the fact that the model is predicting (and Figure 6 is showing) that as impact velocity increases, the amount of energy associated with the movement of the near debris cloud remains rather large compared to the initial impact energy. It would be expected that as velocity increases, the projectile would eventually just perforate the near propellant simulant material without creating a debris cloud (i.e. a 'clean' perforation). This then is at least one area of the model that needs to be addressed in subsequent studies of impact energy partitioning.

7.0 CONCLUSIONS AND RECOMMENDATIONS

In this study, a first-principles-based mathematical model was developed to determine the partitioning of the kinetic energy of an impacting projectile among various solid rocket motor failure modes. Failure modes considered in the analyses included near and far case perforation, near and far case delamination, and fragmentation of the propellant simulant material. Energies involved in material fragmentation were calculated using a fragmentation scheme based on a procedure developed in a previous impact study utilizing propellant simulant materials. Two impact scenarios were considered. In the first, the impact velocity is sufficiently high so that the projectile perforates the near case and propellant simulant layers, but not high enough so that it can perforate the far case and simulant material layers. In the second, the impact velocity is high enough so that the projectile is able to perforate both sides of the rocket motor and exit with some residual kinetic energy. The complexity of the problem required certain assumptions and simplifications to bring the problem down to solvable proportions.

The resulting model was found to be capable of predicting a variety of response characteristics of analog solid rocket motors under high speed projectile impact. Worthy of note is the fact that the model correctly predicted the ballistic limit of the graphite/epoxy case and the propellant simulant materials. For the most part, the numerical results generated with the model over a wide range of impact velocities showed trends that would be expected. Naturally, since the model was developed without any experimental validation, the next step would be to perform a series of tests that would ultimately either validate the model or highlight its weak points. Experimental test results are also required for the selection of appropriate values of the various user-controlled parameters employed in the development of this model.

8.0 ACKNOWLEDGMENTS

The author is grateful to Dr. Ben Thomas and the U.S. Army Space & Strategic Defense Command for the support provided through contract DASG60-89-C-0129/TE-12. The author also thanks Ms. Jamie Fisher of the U.S. Army Missile Command Propulsion Directorate and Dr. Tom Neely of the University of Alabama in Huntsville Research Institute for their assistance during the course of this project.

9.0 REFERENCES

1. Bullet and Fragment Impact Hazards to Solid Rocket Motors, CPIA Report No. SP 92-06, Washington, D.C., 1992.

2. Yuan, W., Goldsmith, W., Radin, J., and Tauber, Z., "Response of Simulated Propellant and Explosives to Projectile Impact -- I. Material Behavior and Penetration Studies", Int. J. Impact Engng., Vol. 12, No. 4, pp. 475-497, 1992.

3. Yuan, W., and Goldsmith, W., "Response of Simulated Propellant and Explosives to Projectile Impact -- II. Fragmentation", Int. J. Impact Engng., Vol. 12, No. 4, pp. 475-497, 1992.

4. Yuan, W., and Goldsmith, W., "Response of Simulated Propellant and Explosives to Projectile Impact -- III. Experimental and Numerical Results of Warhead Penetration and Fragmentation", Int. J. Impact Engng., Vol. 12, No. 4, pp. 475-497, 1992.

5. DeMay, S.C., "An Overview of the U.S. Navy IMAD Propellant Technology Initiatives", in Bullet and Fragment Impact Hazards to Solid Rocket Motors, CPIA Report No. SP 92-06, Washington, D.C., 1992, pp. 89-106.

6. Lindfors, A.J., Schulz, J.C., and Finnegan, S.A., "Plate Curvature Effects on Ballistic Limit and Fragmentation", in Proceedings of the 12th Internation Ballistics Symposium, San Antonio, Texas, October 29 to November 1, 1990, Vol. 3, pp. 159-167.

7. Conkwright, N.B., Introduction to the Theory of Equations, Ginn and Co., New York, 1957.

8. Awerbuch, J., "A Mechanics Approach to Projectile Penetration", Israel J. of Tech., Vol. 8, No. 4, 1970, pp. 375-383.

9. Pierson, M.O., Delfosse, D., Vaziri, R., and Poursartip, A., "Penetration of Laminated Composite Plates Due to Impact", in Proceedings of the 14th International Ballistics Symposium, Quebec, Canada, September 26-29, 1993, Vol. 2, pp. 351-360.

10. Malvern, L.E., Sierakowski, R.L., Ross, C.A., and Cristescu, N., "Impact Failure Mechanisms in Fiber-Reinforced Composite Plates", in High Velocity Deformation of Solids, IUTAM Symposium, Tokyo, Japan, August, 1977, pp. 120-130.

11. Abrate, S., "Impact on Laminated Composite Materials", Appl. Mech. Rev., Vol. 44, No. 4, 1991, pp. 155-190.

12. Mastin, L.A., Results from Mechanical Property Testing of an Inert Minimum Smoke Propellant Simulant, Letter Report RD-PR-93-13, U.S. Army Missile Command, Redstone Arsenal, AL, February, 1993.

13. Littlefield, D., A Study of Shock Mitigation Using Numerical Simulations of Propellant Case Designs, Report No. CR-RD-PR-92-3, U.S. Army Missile Command, Redstone Arsenal, AL, September, 1992.

14. Lundstrom, E., "Shock Sensitivity Testing and Analysis for a Minimum Smoke Propellant", in Bullet and Fragment Impact Hazards to Solid Rocket Motors, CPIA Report No. SP 92-06, Washington, D.C., 1992, pp. 61-76.

15. Curran, D.R., Seaman, L., and Shockey, D.A., "Dynamic Failure of Solids", Physics Reports, Vol. 147, Nos. 5&6, 1987, pp. 253-388.

16. Seaman, L., Curran, D.R., and Murri, W., "A Continuum Model for Dynamic Tensile Microfracture and Fragmentation", J. Appl. Mech., Vol. 52, No. 3, 1985, pp. 593-600.

17. Hudson, F., Covino, J., Finnegan, S.A., and Pringle, J.K., "The Effect of Impact Damage on Solid Propellant Sensitivity to Electrostatic Discharge", in Proceedings of the 1992 JANNAF Propulsion Systems Hazards Subcommittee Meeting, Naval Surface Warfare Center, Maryland, April 27 to May 1, 1992, Vol. 1, pp. 35-40.

18. Atwood, A.I., Price, C.F., Boggs, T.L., "A Comparison of Radiant Ignition and Ballistic Impact Chamber Results", in Proceedings of the 1992 JANNAF Propulsion Systems Hazards Subcommittee Meeting, Naval Surface Warfare Center, Maryland, April 27 to May 1, 1992, Vol. 1, pp. 209-226.

19. Heimdahl, O.E.R., and Dimaranan, L.F., "Study of Imapct-Induced Detonation for Steel and Titanium Covered PBXN-107", in Proceedings of the 1992 JANNAF Propulsion Systems Hazards Subcommittee Meeting, Naval Surface Warfare Center, Maryland, April 27 to May 1, 1992, Vol. 1, pp. 209-226.

20. Murray, Y.D., Impact Response of Kevlar/Epoxy Rings with Damage, DNA-TR-90-159, Alexandria, VA, March, 1991.

21. Wang, C.Y., and Yew, C.H., "Impact Damage in Composite Laminates", Computers and Structures, Vol. 37, No. 6, 1990, pp. 967-982.

22. Razi, H., and Kobayashi, A.S., "Delamination in Cross-Ply Laminated Composites Subjected to Low Velocity Impact", AIAA Journal, Vol. 31, No. 8, 1993, pp 1498-1504.

23. Larom, D., Herakovich, C.T., and Aboudi, J., "Dynamic Response of Pulse Loaded Laminated Composite Cylinders", Int. J. Impact Engng., Vol. 11, No. 2, 1991, pp. 233-248.

24. Refsneider, K.L., Henneke, E.G., and Stinchcomb, W.W., "Delamination in Quasi-isotropic Graphite/epoxy Laminates", ASTM STP 617, 1977, pp. 93-105.

25. Crossman, F.W., Warren, W.J., Wand, A.S.D.,and Law, G.E., "Initiation and Growth of Transverse Cracks and Edge Delaminations in Composite Laminates", J. Comp. Matls., Vol. 14, 1980, pp. 88-108.

26. Bostaph, G.M., and Elber, W., "A Fracture Mechanics Analysis for Delamination Growth During Impact on Composite Plates", ASME AD-06, 1983, pp. 133-138.

27. Kinslow, R., High Velocity Impact Phenomena, Academic Press, 1970.

APPENDIX A -- FORTRAN 77 SOURCE CODE

```
      PROGRAM IMEDEL
      IMPLICIT DOUBLE PRECISION (A-H,O-Z)
      DOUBLE PRECISION LP,NL,K1D,KPR,KPS,MP,MDC
      CHARACTER*1 OPT
      OPEN(1,FILE='IMDATA',STATUS='UNKNOWN')
      OPEN(2,FILE='EDELOUT',STATUS='UNKNOWN')
C
C     READ MATERIAL AND IMPACT PARAMTERS ...
C           RHOPR ..... PROJECTILE DENSITY (KG/M^3)
C           RP ........ PROJECTILE RADIUS (CM)
C           LP ........ PROJECTILE LENGTH (CM)
C           KPR ....... PROJECTILE BULK MODULUS (N/M^2)
C           SPR ....... SLOPE OF PROJECTILE US-UP CURVE
C           VP ........ IMPACT VELOCITY (FT/SEC)
C           NL ........ NUMBER OF LAYERS IN GR/EP CASE
C           TL ........ LAYER THICKNESS IN GR/EP CASE
C           SIGUGE ..... GR/EP ULT STRENGTH (N/M^2)
C           RHOGE ..... GR/EP DENSITY (KG/M^3)
C           GC ........ PRP SIM MATL CRIT ENERGY REL (N/M^2)
C           RHOPS ..... PRP SIM MATL DENSITY (KG/M^3)
C           K1D ....... PRP SIM MATL MODE-I SIF (PA-/M)
C           KPS ....... PRP SIM MATL BULK MODULUS (N/M^2)
C           SPS ....... PRP SIM MATL US-UP CURVE SLOPE
C           THC,THC1 ... PRP SIM MATL CONE ANGLES (DEG)
C           AMIN ...... PRP SIM MATL MIN FRAG SIZE (MM)
C           H ......... PRP SIM MATL THICKNESS (CM)
C           SIGUPS ..... PRP SIM MATL ULT STRENGTH (N/M^2)
C
      READ(1,5) RHOPR,RP,LP,KPR,SPR,VP1
    5  FORMAT(3F10.5,E10.3,2F10.5)
      READ(1,6) NL,TL,SIGUGE,RHOGE,GC
    6  FORMAT(2F10.5,E10.3,2F10.5)
      READ(1,7) RHOPS,K1D,KPS,SPS,THC,THC1,AMIN,H,SIGUPS
    7  FORMAT(F10.5,2E10.3,F10.5,2F5.2,2F10.5,E10.3)
      READ(1,8) OPT
    8  FORMAT(A1)
C
C     CONVERT ALL THICKNESS TO M, SPEEDS TO M/SEC, AND MASSES TO KG
C
      RP=RP/100.0
      LP=LP/100.0
      VP=VP1*0.3048
      TL=TL/1000.0
      AMIN=AMIN/1000.0
      H=H/100.0
C
      PI=3.141592
C
      AH=PI*RP*RP
      MP=PI*RHOPR*RP*RP*LP
      EINIT=MP*VP*VP/2.0
C
      TGE=NL*TL
      D=MP/(RHOGE*AH)
      T1=D/(TGE+D)
      T2=(2.0*SIGUGE)/(3.0*RHOGE)
      VBL=DSQRT(T2*(1.0/(T1*T1*T1)-1.0))
C
      IF (VBL.GE.VP) THEN
      WRITE(2,50) VP,VBL
   50 FORMAT('THE SPECIFIED IMPACT VELOCITY (',F6.1,' M/S) IS LESS THAN
     $THE CALCULATED',/,'BALLISTIC LIMIT VELOCITY (',F6.1' M/S) OF THE G
     $R/EP CASE.',///,'***** PROGRAM TERMINATED *****')
      STOP
```

```
      ENDIF
C
      EPERFGE=MP*VBL*VBL/2.0
C
      AM=9.0*AH
      T3=1.0-DEXP(-VP/VBL)
      EDELGE=AM*GC*(NL-1.0)*T3
C
      CPS=DSQRT(KPS/RHOPS)
      D1=MP/(RHOPS*AH)
      T4=D1/(H+D1)
      T5=(2.0*SIGUPS)/(3.0*RHOPS)
      UBL=DSQRT(T5*(1.0/(T4*T4*T4)-1.0))
      VF=DSQRT((VP*VP+T2)*(T1*T1*T1)-T2)
      H1=H*DEXP((1.0-VF/UBL)/4.0)
      RC=(H-H1)*DTAN(PI*THC/180.0)
      G1=2.0*(AMIN*AMIN*AMIN)/27.0
      G2=(3.0/8.0)*((RC*RC)*(H-H1)/3.0+(RP*RP)*H1)
      GG=-G1-G2
      HH=-AMIN*AMIN/9.0
      DISC=GG*GG+4.0*HH*HH*HH
      T6=(-GG+DSQRT(DISC))/2.0
      T7=(-GG-DSQRT(DISC))/2.0
      AX1=T6**(1.0/3.0)
      AX2=T7**(1.0/3.0)
      AMAX=AX1+AX2-AMIN/3.0
      ACOEF=(3.0/8.0)*(RC*RC*(H-H1)/3.0+RP*RP*H1)/(AMAX-AMIN)
      PSVOL=(8.0/3.0)*PI*ACOEF*(AMAX-AMIN)
      T8=(K1D*K1D)/(2.0*RHOPS*CPS*CPS)
      T9=(8.0/3.0)*G2/(AMAX-AMIN)
      T10=DSQRT(RC*RC+(H-H1)*(H-H1))
      EFRAGCR=T8*(5.0*PI*T9*DLOG(AMAX/AMIN)+PI*RC*T10)
C
      MDC=(PI*RHOPS/3.0)*RC*RC*(H-H1)+RHOPS*RP*RP*H1
      CPR=DSQRT(KPR/RHOPR)
      RHORAT=RHOPS/RHOPR
      AA=SPR-SPS*RHORAT
      BB=2.0*SPR*VF+CPR+CPS*RHORAT
      CC=CPR*VF+SPR*VF*VF
      DPP=BB*BB-4.0*AA*CC
      UP=(BB-DSQRT(DPP))/(2.0*AA)
      EDELIV=PI*(RP*RP*RHOPS*(H/2.0))*(2.0*UP)*(2.0*UP)/2.0
      EFRAGMV=EDELIV-EFRAGCR
      VDC=DSQRT(2.0*EFRAGMV/MDC)
C
      EPROJR=EINIT-EPERFGE-EDELGE-EFRAGCR-EFRAGMV
      VR=DSQRT(2.0*EPROJR/MP)
C
      IF (OPT.EQ.'L') GOTO 100
C
      H11=H*DEXP((1.0-VR/UBL)/4.0)
      RC1=(H-H11)*DTAN(PI*THC1/180.0)
      G11=G1
      G21=(3.0/8.0)*((RC1*RC)*(H-H11)/3.0+(RP*RP)*H11)
      GG1=-G11-G21
      HH1=HH
      DISC2=GG1*GG1+4.0*HH1*HH1*HH1
      T61=(-GG1+SQRT(DISC2))/2.0
      T71=(-GG1-SQRT(DISC2))/2.0
      AX11=T61**(1.0/3.0)
      AX21=T71**(1.0/3.0)
      AMAX1=AX11+AX21-AMIN/3.0
      ACOEF1=(3.0/8.0)*(RC1*RC1*(H-H11)/3.0+RP*RP*H11)/(AMAX1-AMIN)
      PSVOL1=(8.0/3.0)*PI*ACOEF1*(AMAX1-AMIN)
```

```
      T81=T8
      T91=(8.0/3.0)*G21/(AMAX1-AMIN)
      T101=DSQRT(RC1*RC1+(H-H11)*(H-H11))
      EFRGCR=T81*(5.0*PI*T91*DLOG(AMAX1/AMIN)+PI*RC1*T101)
C
      VI=DSQRT(VR*VR-EFRGCR/(MP/2.0))
      EDLGE=AM*GC*(NL-1.0)*(1.0-DEXP(-VI/VBL))
C
      IF (VI.LT.VBL) THEN
      EPROJF=0.0
      ENDIF
      IF (VI.GT.VBL) THEN
      EPROJF=EPROJR-EFRGCR-EPERFGE-EDLGE
      ENDIF
      VRF=DSQRT(EPROJF/(MP/2.0))
C
  100 WRITE(2,101)
  101 FORMAT(/,'IMPACT ENERGY PARTITIONING FOR CYLINDRICAL FRAGMENT',
     $/,'IMPACT ON A FILAMENT-WOUND CASE WITH PROPELLANT SIMULANT ...')
C
      RHOPR=RHOPR/1000.0
      RP=RP*100.0
      LP=LP*100.0
      MP=MP*1000.0
      WRITE(2,102) RHOPR,KPR,SPR,CPR,RP,LP,MP,VP,VP1
  102 FORMAT(/,'PROJECTILE PROPERTIES ...',/,5X,'DENSITY ...',F10.3,
     $' GM/CM^3',/,5X,'BULK MODULUS ...',E10.3,' N/M^2',/,5X,'US-UP SLOP
     $E ....',F10.3,/,5X,'AD SOUND SP ....',F10.3,' M/SEC',/,5X,'RADIUS
     $.....',F10.3,' CM',/,5X,'LENGTH .....',F10.3,' CM',/,5X,
     $'MASS .....',F10.3,' GM',/,5X,'IMP VEL .....',F10.3,
     $' M/SEC = ',F10.3,' FT/SEC')
C
      RHOGE=RHOGE/1000.0
      TL=TL*1000.0
      TGE=TGE*1000.0
      WRITE(2,103) RHOGE,NL,TL,TGE,SIGUGE,GC,VBL
  103 FORMAT('GR/EP CASE PROPERTIES ...',/,5X,'DENSITY .............',
     $F10.3,' GM/CM^3',/,5X,'# LAYERS .............',F10.3,/,5X,'LAYER T
     $HKNESS .....',F10.3,' MM',/,5X,'TOTAL THKNESS .....',F10.3,
     $' MM',/,5X,'ULT STRENGTH .....',E10.3,' N/M^2',/,5X,'CRIT ENER
     $ REL RATE ...',F10.3,' N/M^2',/,5X,'BALL LIM VEL .....',F10.3,
     $' M/SEC')
C
      RHOPS=RHOPS/1000.0
      AMIN=AMIN*1000.0
      H=H*100.0
      WRITE(2,104) RHOPS,K1D,KPS,SPS,CPS,SIGUPS,AMIN,H,UBL
  104 FORMAT('PROPELLANT SIMULANT MATERIAL PROPERTIES ...',/,5X,
     $'DENSITY .....',F10.3,' GM/CM^3',/,5X,'DYN FRACT STR ...',
     $E10.3,' N/M^2',/,5X,'BULK MODULUS ....',E10.3,' N/M^2',/,5X,'US-UP
     $ SLOPE .....',F10.3,/,5X,'AD SOUND SP .....',F10.3,' M/SEC',/,5X,
     $'ULT STRENGTH ....',E10.3,' N/M^2',/,5X,'MIN FRAG SIZE ...',
     $F10.3,' MM',/,5X,'THICKNESS .....',F10.3,' CM',/,5X,'BALL LIM VE
     $L ....',F10.3,' M/SEC')
C
      H1=H1*100.0
      HC=H-H1
      RC=RC*100.0
      MDC=MDC*1000.0
      AMAX=AMAX*100.0
      ACOEF=ACOEF*100.0*100.0
      PSVOL=PSVOL*100.0*100.0*100.0
      WRITE(2,105) EINIT,EPERFGE,VF,EDELGE,EDELIV,EFRAGCR,ACOEF,AMAX,
     $RC,HC,THC,PSVOL,MDC,UP,EFRAGMV,VDC,EPROJR,VR
```

```
  105 FORMAT(/,'ENERGY PARTITIONING DUE TO FIRST WALL PERFORATION ...',/
     $,5X,'INITIAL PROJECTILE KINETIC ENERGY ..........',F10.3,' J',/
     $,5X,'ENERGY REQD TO PERF GR/EP CASE .............',F10.3,' J',/,
     $10X,'RES PRJ VEL GR/EP PERF .......',F10.3,' M/SEC',/
     $,5X,'ENERGY ABS IN GR/EP DELAMINATION ...........',F10.3,' J',/
     $,5X,'ENERGY DELIVERED TO PRP SIM MATL ...........',F10.3,' J',/,
     $,5X,'ENERGY REQD TO FRAG PRP SIM MATL ...........',F10.3,' J',/,
     $10X,'CUM FRAG FCN COEFFICIENT .....',F10.3,' CM^2',/,
     $10X,'MAX PRP SIM MATL FRAG DIA ....',F10.3,' CM',/,
     $10X,'PRP SIM MATL CONE PLUG RAD ...',F10.3,' CM',/,
     $10X,'PRP SIM MATL CONE PLUG HT ....',F10.3,' CM',/,
     $10X,'PRP SIM MATL CONE 1/2-ANG ....',F10.3,' DEG',/,
     $10X,'PRP SIM MATL FRAG VOLUME .....',F10.3,' CM^3',/,
     $10X,'PRP SIM MATL DEB CLD MASS ....',F10.3,' GM',/,
     $10X,'PRP SIM MATL PARTICLE VEL ....',F10.3,' M/SEC',/,
     $5X,'ENERGY AVAIL TO MV PRP SIM MATL DEB CLD ....',F10.3,' J',/,
     $10X,'PRP SIM MATL DEB CLD VEL .....',F10.3,' M/SEC',/
     $,5X,'RESIDUAL PROJECTILE KINETIC ENERGY .........',F10.3,' J',/,
     $10x,'RESID PROJ VELOCITY ..........',F10.3,' M/SEC')
C
      F1=EPERFGE/EINIT
      F2=EDELGE/EINIT
      F3=EFRAGCR/EINIT
      F4=EFRAGMV/EINIT
      F5=EPROJR/EINIT
C
      WRITE(2,106) F1,F2,F3,F4,F5
  106 FORMAT(/,'EPERFGE/EINIT = ',F10.3,/,'EDELGE/EINIT  = ',F10.3,
     $/,'EFRAGCR/EINIT = ',F10.3,/,'EFRAGMV/EINIT = ',F10.3,/,
     $'EPROJR/EINIT  = ',F10.3)
      IF (OPT.EQ.'L') THEN
      FS=F1+F2+F3+F4+F5
      WRITE(2,107) FS
  107 FORMAT('SUM OF RATIOS = ',F10.3,/)
      IF (VR.GT.VBL) WRITE(2,108)
  108 FORMAT('***** WARNING ***** RESID PROJ VEL EXCEEDS BALLISTIC LIMIT
     $ OF',/,'REAR GR/EP CASE WALL.  RERUN USING HIGH VELOCITY OPTION.')
      GOTO 200
      ENDIF
C
      H11=H11*100.0
      HC1=H-H11
      RC1=RC1*100.0
      AMAX1=AMAX1*100.0
      ACOEF1=ACOEF1*100.0*100.0
      PSVOL1=PSVOL1*100.0*100.0*100.0
      WRITE(2,150) EPROJR,EFRGCR,ACOEF1,AMAX1,RC1,HC1,THC1,PSVOL1,VI,
     $EDLGE,EPERFGE,EPROJF,VRF
  150 FORMAT(/,'ENERGY PARTITIONING DUE TO SECOND WALL PERFORATION ...',
     $/,5X,'RESID PROJ KIN ENERGY AFTER 1ST WALL PERF ....',F10.3,' J',
     $/,5X,'ENERGY REQD TO FRAG PRP SIM MATL .............',F10.3,' J',/,
     $10X,'PRP SIM MATL FRAG FCN COEFF .......',F10.3,' CM^2',/,
     $10X,'MAX PRP SIM MATL FRAG DIA .........',F10.3,' J',/,
     $10X,'PRP SIM MATL PLUG CONE RAD ........',F10.3,' CM',/,
     $10X,'PRP SIM MATL PLUG CONE HT .........',F10.3,' CM',/
     $10X,'PRP SIM MATL CONE 1/2-ANG .........',F10.3,' DEG',/,
     $10X,'PRP SIM MATL FRAG VOLUME ..........',F10.3,' CM^3',/,
     $10X,'POST PRP SIM MATL FRAG PROJ VEL ...',F10.3,' M/SEC',/
     $,5X,'ENERGY ABS BY IN GR/EP DELAMINATION ...........',F10.3,' J',/
     $,5X,'ENERGY REQD TO PERF GR/EP CASE ................',F10.3,' J',/
     $,5X,'FINAL RESIDUAL PROJECTILE KINETIC ENERGY ......',F10.3,' J',/,
     $10X,'FINAL RES PROJ VEL ............',F10.3,' M/SEC')
C
      F6=EFRGCR/EINIT
```

```
      F7=EDLGE/EINIT
      F8=EPERFGE/EINIT
      F9=EPROJF/EINIT
      FS=F1+F2+F3+F4+F6+F7+F8+F9
      WRITE(2,151) F6,F7,F8,F9,FS
  151 FORMAT(/,'EFRCCR/EINIT  = ',F10.3,/,'EDLGE/EINIT   = ',F10.3,/,
     $'EPERFGE/EINIT = ',F10.3,/,'EPROJF/EINIT  = ',F10.3,/,'SUM OF RATI
     $OS = ',F10.3)
C
  200 STOP
      END
```

APPENDIX B -- SAMPLE INPUT AND OUTPUT FILES

Sample Input File IMDATA ...

```
    7830.0        0.5        2.0   1.635E+11        1.55     11000.0
      6.0        0.4   0.200E+10     1530.0       400.0
    1780.0  0.128E+07  0.817E+10       1.95  45.0  45.0        0.1        2.54  0.590E+07
H
```

Sample Output File for a Low Velocity Impact ...

```
IMPACT ENERGY PARTITIONING FOR CYLINDRICAL FRAGMENT
IMPACT ON A FILAMENT-WOUND CASE WITH PROPELLANT SIMULANT ...

PROJECTILE PROPERTIES ...
     DENSITY ...      7.830 GM/CM^3
     BULK MODULUS ... 0.164E+12 N/M^2
     US-UP SLOPE ....     1.550
     AD SOUND SP ....  4569.598 M/SEC
     RADIUS .........     0.500 CM
     LENGTH .........     2.000 CM
     MASS ...........    12.299 GM
     IMP VEL ........   304.800 M/SEC =   1000.000 FT/SEC

GR/EP CASE PROPERTIES ...
     DENSITY ..............     1.530 GM/CM^3
     # LAYERS .............     6.000
     LAYER THKNESS ........     0.400 MM
     TOTAL THKNESS ........     2.400 MM
     ULT STRENGTH ......... 0.200E+10 N/M^2
     CRIT ENER REL RATE ...   400.000 N/M^2
     BALL LIM VEL .........   250.502 M/SEC

PROPELLANT SIMULANT MATERIAL PROPERTIES ...
     DENSITY .........     1.780 GM/CM^3
     DYN FRACT STR ... 0.128E+07 N/M^2
     BULK MODULUS .... 0.817E+10 N/M^2
     US-UP SLOPE .....     1.950
     AD SOUND SP .....  2142.402 M/SEC
     ULT STRENGTH .... 0.590E+07 N/M^2
     MIN FRAG SIZE ...     0.100 MM
     THICKNESS .......     2.540 CM
     BALL LIM VEL ....    50.196 M/SEC

ENERGY PARTITIONING DUE TO FIRST WALL PERFORATION ...
     INITIAL PROJECTILE KINETIC ENERGY ..........   571.323 J
     ENERGY REQD TO PERF GR/EP CASE .............   385.900 J
          RES PRJ VEL GR/EP PERF .......   167.709 M/SEC
     ENERGY ABS IN GR/EP DELAMINATION ...........     0.995 J
     ENERGY DELIVERED TO PRP SIM MATL ...........    79.568 J
     ENERGY REQD TO FRAG PRP SIM MATL ...........     0.884 J
          CUM FRAG FCN COEFFICIENT .....     0.468 CM^2
          MAX PRP SIM MATL FRAG DIA ....     0.674 CM
          PRP SIM MATL CONE PLUG RAD ...     1.125 CM
          PRP SIM MATL CONE PLUG HT ....     1.125 CM
          PRP SIM MATL CONE 1/2-ANG ....    45.000 DEG
          PRP SIM MATL FRAG VOLUME .....     2.603 CM^3
          PRP SIM MATL DEB CLD MASS ....     3.286 GM
          PRP SIM MATL PARTICLE VEL ....   149.691 M/SEC
     ENERGY AVAIL TO MV PRP SIM MATL DEB CLD ....    78.684 J
          PRP SIM MATL DEB CLD VEL .....   218.842 M/SEC
     RESIDUAL PROJECTILE KINETIC ENERGY .........   104.860 J
          RESID PROJ VELOCITY ..........   130.581 M/SEC

EPERFGE/EINIT =      0.675
EDELGE/EINIT  =      0.002
EFRAGCR/EINIT =      0.002
EFRAGMV/EINIT =      0.138
EPROJR/EINIT  =      0.184
SUM OF RATIOS =      1.000
```

Sample Output File for a Medium Velocity Impact ...

```
IMPACT ENERGY PARTITIONING FOR CYLINDRICAL FRAGMENT
IMPACT ON A FILAMENT-WOUND CASE WITH PROPELLANT SIMULANT ...

PROJECTILE PROPERTIES ...
     DENSITY ...      7.830 GM/CM^3
     BULK MODULUS ... 0.164E+12 N/M^2
     US-UP SLOPE ....     1.550
     AD SOUND SP ....  4569.598 M/SEC
     RADIUS .........     0.500 CM
     LENGTH .........     2.000 CM
     MASS ...........    12.299 GM
     IMP VEL ........   609.600 M/SEC =   2000.000 FT/SEC

GR/EP CASE PROPERTIES ...
     DENSITY ..............     1.530 GM/CM^3
     # LAYERS .............     6.000
     LAYER THKNESS ........     0.400 MM
     TOTAL THKNESS ........     2.400 MM
     ULT STRENGTH ......... 0.200E+10 N/M^2
     CRIT ENER REL RATE ...   400.000 N/M^2
     BALL LIM VEL .........   250.502 M/SEC

PROPELLANT SIMULANT MATERIAL PROPERTIES ...
     DENSITY .........     1.780 GM/CM^3
     DYN FRACT STR ... 0.128E+07 N/M^2
     BULK MODULUS .... 0.817E+10 N/M^2
     US-UP SLOPE .....     1.950
     AD SOUND SP .....  2142.402 M/SEC
     ULT STRENGTH .... 0.590E+07 N/M^2
     MIN FRAG SIZE ...     0.100 MM
     THICKNESS .......     2.540 CM
     BALL LIM VEL ....    50.196 M/SEC

ENERGY PARTITIONING DUE TO FIRST WALL PERFORATION ...
     INITIAL PROJECTILE KINETIC ENERGY .....  2285.291 J
     ENERGY REQD TO PERF GR/EP CASE .....      385.900 J
          RES PRJ VEL GR/EP PERF .....   536.763 M/SEC
     ENERGY ABS IN GR/EP DELAMINATION .....      1.290 J
     ENERGY DELIVERED TO PRP SIM MATL .....    775.711 J
     ENERGY REQD TO FRAG PRP SIM MATL .....      2.969 J
          CUM FRAG FCN COEFFICIENT .....     1.367 CM^2
          MAX PRP SIM MATL FRAG DIA ....     1.159 CM
          PRP SIM MATL CONE PLUG RAD ...     2.315 CM
          PRP SIM MATL CONE PLUG HT ....     2.315 CM
          PRP SIM MATL CONE 1/2-ANG ....    45.000 DEG
          PRP SIM MATL FRAG VOLUME .....    13.167 CM^3
          PRP SIM MATL DEB CLD MASS ....    23.223 GM
          PRP SIM MATL PARTICLE VEL ....   467.389 M/SEC
     ENERGY AVAIL TO MV PRP SIM MATL DEB CLD ....   772.742 J
          PRP SIM MATL DEB CLD VEL .....   257.973 M/SEC
     RESIDUAL PROJECTILE KINETIC ENERGY .....  1122.391 J
          RESID PROJ VELOCITY .....   427.215 M/SEC

EPERFGE/EINIT =      0.169
EDELGE/EINIT  =      0.001
EFRAGCR/EINIT =      0.001
EFRAGMV/EINIT =      0.338
EPROJR/EINIT  =      0.491
```

```
ENERGY PARTITIONING DUE TO SECOND WALL PERFORATION ...
     RESID PROJ KIN ENERGY AFTER 1ST WALL PERF ....  1122.391 J
     ENERGY REQD TO FRAG PRP SIM MATL .............     2.682 J
          PRP SIM MATL FRAG FCN COEFF .......     1.166 CM^2
          MAX PRP SIM MATL FRAG DIA .........     1.109 J
          PRP SIM MATL PLUG CONE RAD ........     2.152 CM
          PRP SIM MATL PLUG CONE HT .........     2.152 CM
          PRP SIM MATL CONE 1/2-ANG .........    45.000 DEG
          PRP SIM MATL FRAG VOLUME ..........    10.735 CM^3
          POST PRP SIM MATL FRAG PROJ VEL ...   426.704 M/SEC
     ENERGY ABS BY IN GR/EP DELAMINATION ...........     1.156 J
     ENERGY REQD TO PERF GR/EP CASE ................   385.900 J
     FINAL RESIDUAL PROJECTILE KINETIC ENERGY ......   732.652 J
          FINAL RES PROJ VEL ............   345.162 M/SEC

EFRGCR/EINIT  =      0.001
EDLGE/EINIT   =      0.001
EPERFGE/EINIT =      0.169
EPROJF/EINIT  =      0.321
SUM OF RATIOS =      1.000
```

Sample Output File for a High Velocity Impact ...

```
IMPACT ENERGY PARTITIONING FOR CYLINDRICAL FRAGMENT
IMPACT ON A FILAMENT-WOUND CASE WITH PROPELLANT SIMULANT ...

PROJECTILE PROPERTIES ...
     DENSITY ...      7.830 GM/CM^3
     BULK MODULUS ... 0.164E+12 N/M^2
     US-UP SLOPE ....     1.550
     AD SOUND SP ....  4569.598 M/SEC
     RADIUS .........     0.500 CM
     LENGTH .........     2.000 CM
     MASS ...........    12.299 GM
     IMP VEL ........  3352.800 M/SEC =  11000.000 FT/SEC

GR/EP CASE PROPERTIES ...
     DENSITY ..............     1.530 GM/CM^3
     # LAYERS .............     6.000
     LAYER THKNESS ........     0.400 MM
     TOTAL THKNESS ........     2.400 MM
     ULT STRENGTH ......... 0.200E+10 N/M^2
     CRIT ENER REL RATE ...   400.000 N/M^2
     BALL LIM VEL .........   250.502 M/SEC

PROPELLANT SIMULANT MATERIAL PROPERTIES ...
     DENSITY .........     1.780 GM/CM^3
     DYN FRACT STR ... 0.128E+07 N/M^2
     BULK MODULUS .... 0.817E+10 N/M^2
     US-UP SLOPE .....     1.950
     AD SOUND SP .....  2142.402 M/SEC
     ULT STRENGTH .... 0.590E+07 N/M^2
     MIN FRAG SIZE ...     0.100 MM
     THICKNESS .......     2.540 CM
     BALL LIM VEL ....    50.196 M/SEC

ENERGY PARTITIONING DUE TO FIRST WALL PERFORATION ...
     INITIAL PROJECTILE KINETIC ENERGY ..... 69130.046 J
     ENERGY REQD TO PERF GR/EP CASE .............  385.900 J
          RES PRJ VEL GR/EP PERF .......  3229.187 M/SEC
     ENERGY ABS IN GR/EP DELAMINATION ...........    1.414 J
     ENERGY DELIVERED TO PRP SIM MATL ........... 22508.139 J
     ENERGY REQD TO FRAG PRP SIM MATL ...........    3.602 J
          CUM FRAG FCN COEFFICIENT .....     1.630 CM^2
          MAX PRP SIM MATL FRAG DIA ....     1.267 CM
          PRP SIM MATL CONE PLUG RAD ...     2.540 CM
          PRP SIM MATL CONE PLUG HT ....     2.540 CM
          PRP SIM MATL CONE 1/2-ANG ....    45.000 DEG
          PRP SIM MATL FRAG VOLUME .....    17.160 CM^3
          PRP SIM MATL DEB CLD MASS ....    30.546 GM
          PRP SIM MATL PARTICLE VEL ....  2517.666 M/SEC
     ENERGY AVAIL TO MV PRP SIM MATL DEB CLD .... 22504.537 J
          PRP SIM MATL DEB CLD VEL .....  1213.879 M/SEC
     RESIDUAL PROJECTILE KINETIC ENERGY ..... 46234.593 J
          RESID PROJ VELOCITY ..........  2741.939 M/SEC

EPERFGE/EINIT =      0.006
EDELGE/EINIT  =      0.000
EFRAGCR/EINIT =      0.000
EFRAGMV/EINIT =      0.326
EPROJR/EINIT  =      0.669
```

```
ENERGY PARTITIONING DUE TO SECOND WALL PERFORATION ...
     RESID PROJ KIN ENERGY AFTER 1ST WALL PERF .... 46234.593 J
     ENERGY REQD TO FRAG PRP SIM MATL .............      3.602 J
          PRP SIM MATL FRAG FCN COEFF .......      1.630 CM^2
          MAX PRP SIM MATL FRAG DIA .........      1.267 J
          PRP SIM MATL PLUG CONE RAD ........      2.540 CM
          PRP SIM MATL PLUG CONE HT .........      2.540 CM
          PRP SIM MATL CONE 1/2-ANG .........     45.000 DEG
          PRP SIM MATL FRAG VOLUME ..........     17.160 CM^3
          POST PRP SIM MATL FRAG PROJ VEL ...   2741.832 M/SEC
     ENERGY ABS BY IN GR/EP DELAMINATION ............      1.414 J
     ENERGY REQD TO PERF GR/EP CASE .................    385.900 J
     FINAL RESIDUAL PROJECTILE KINETIC ENERGY ...... 45843.678 J
          FINAL RES PROJ VEL .............  2730.323 M/SEC

EFRGCR/EINIT  =      0.000
EDLGE/EINIT   =      0.000
EPERFGE/EINIT =      0.006
EPROJF/EINIT  =      0.663
SUM OF RATIOS =      1.000
```

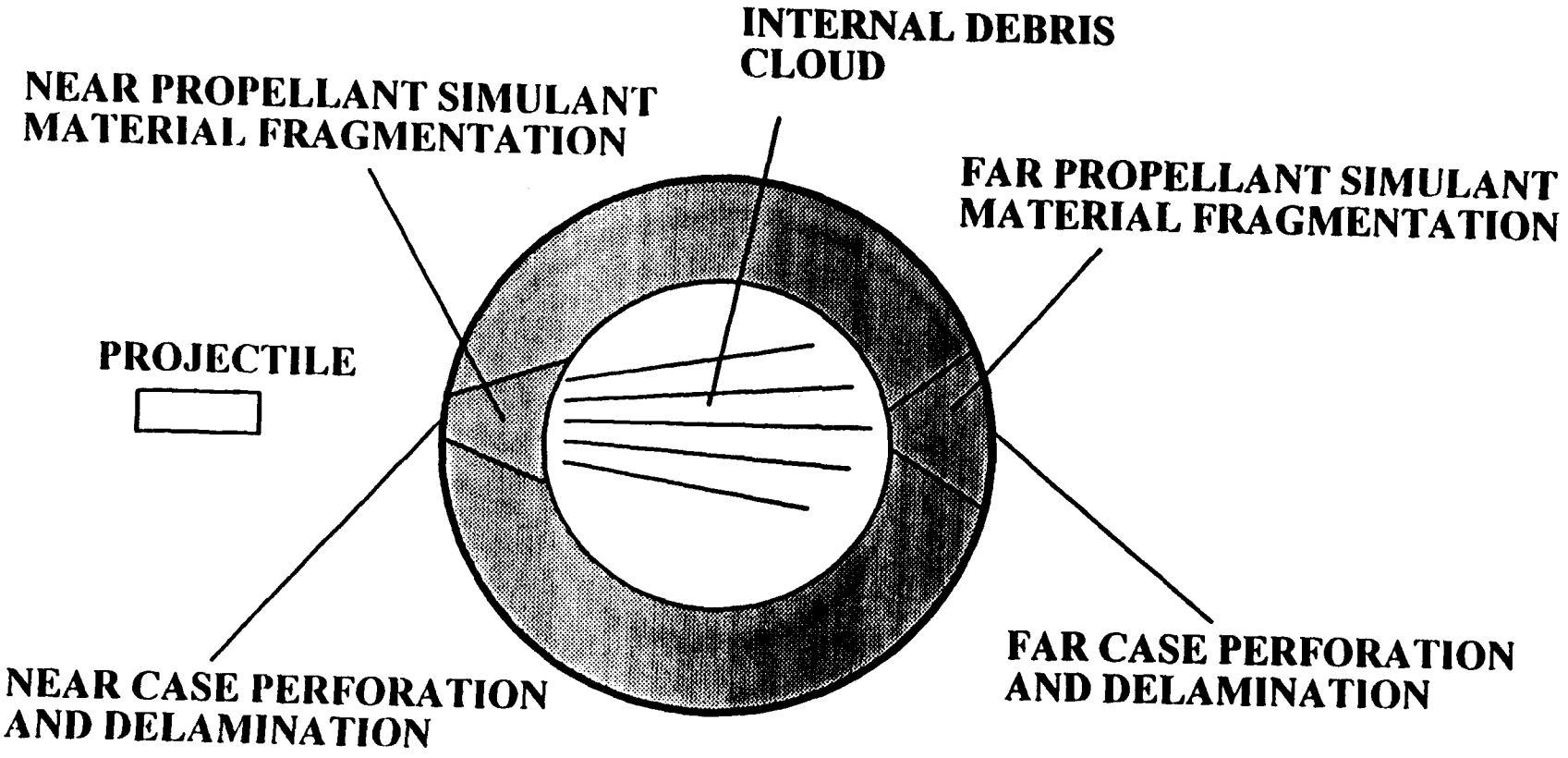

Figure 1. Generic Solid Rocket Motor Impacted by a Cylindrical Projectile

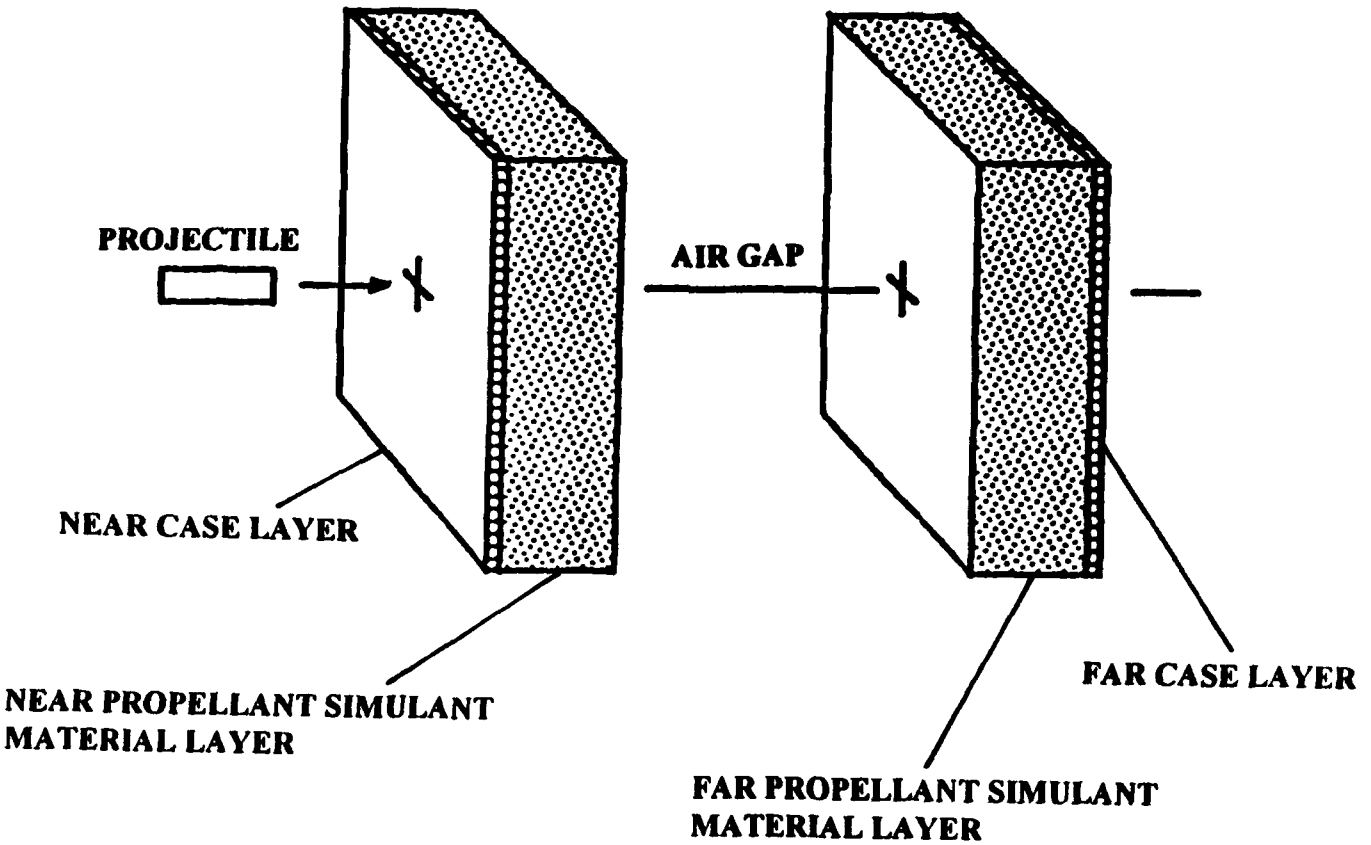

Figure 2. Flat Plate Model of Solid Rocket Motor

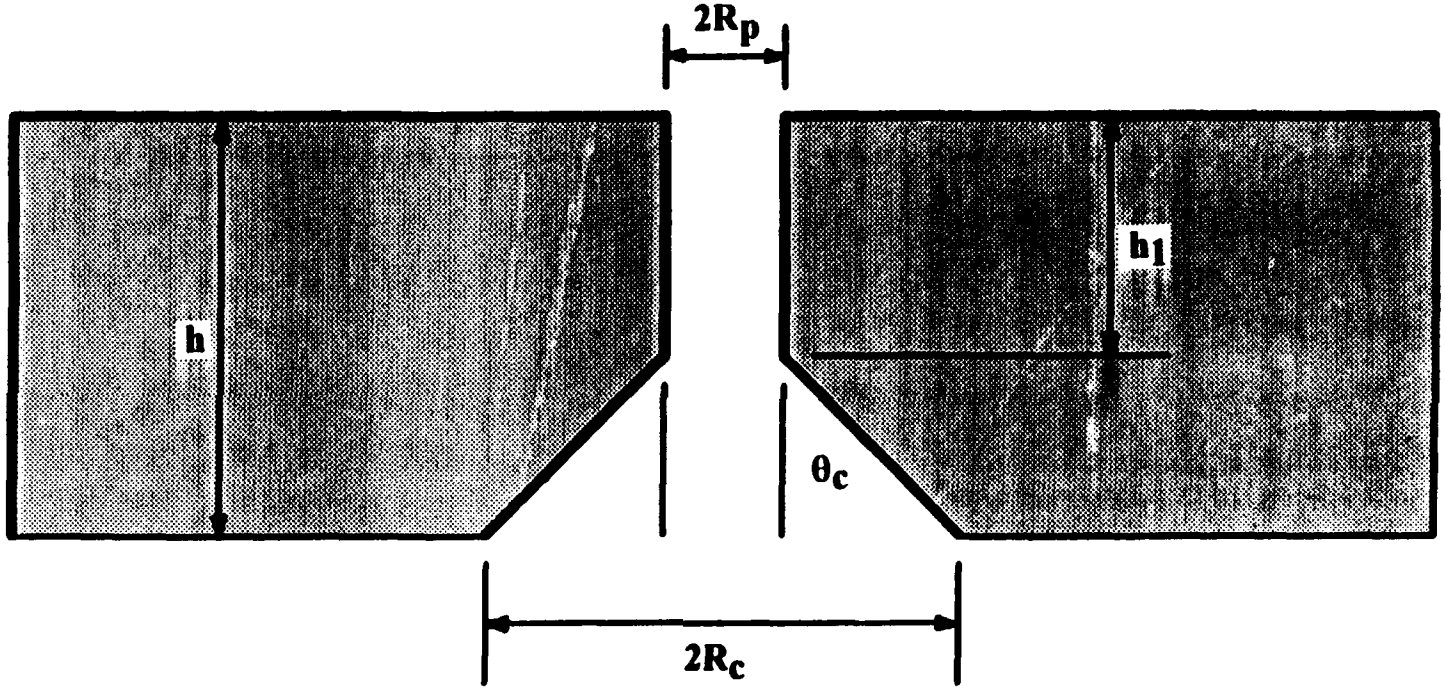

Figure 3. Propellant Simulant Material Cavity Model

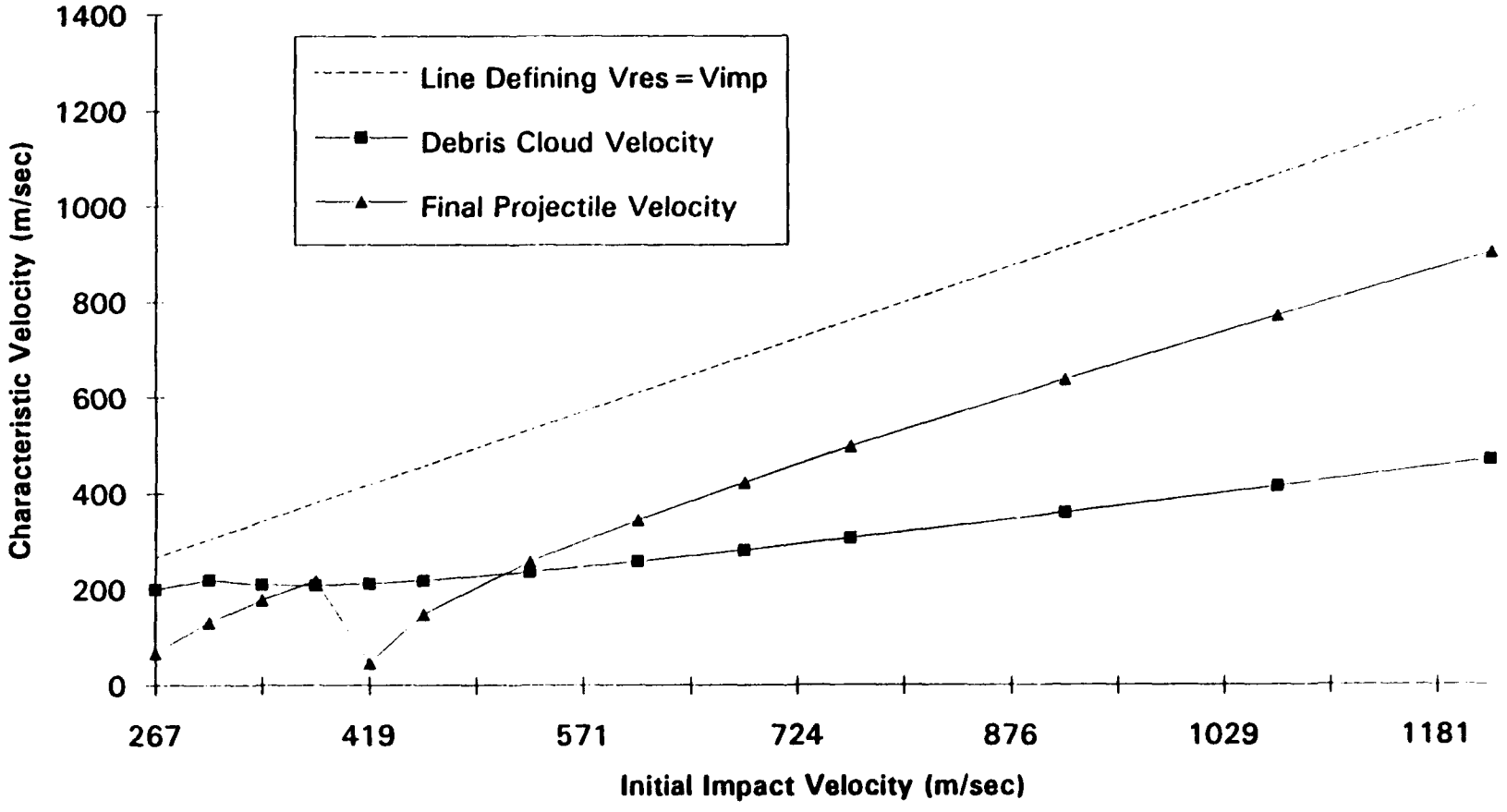

Figure 4. Propellant Simulant Debris Cloud and Final Projectile Velocity vs. Initial Impact Velocity

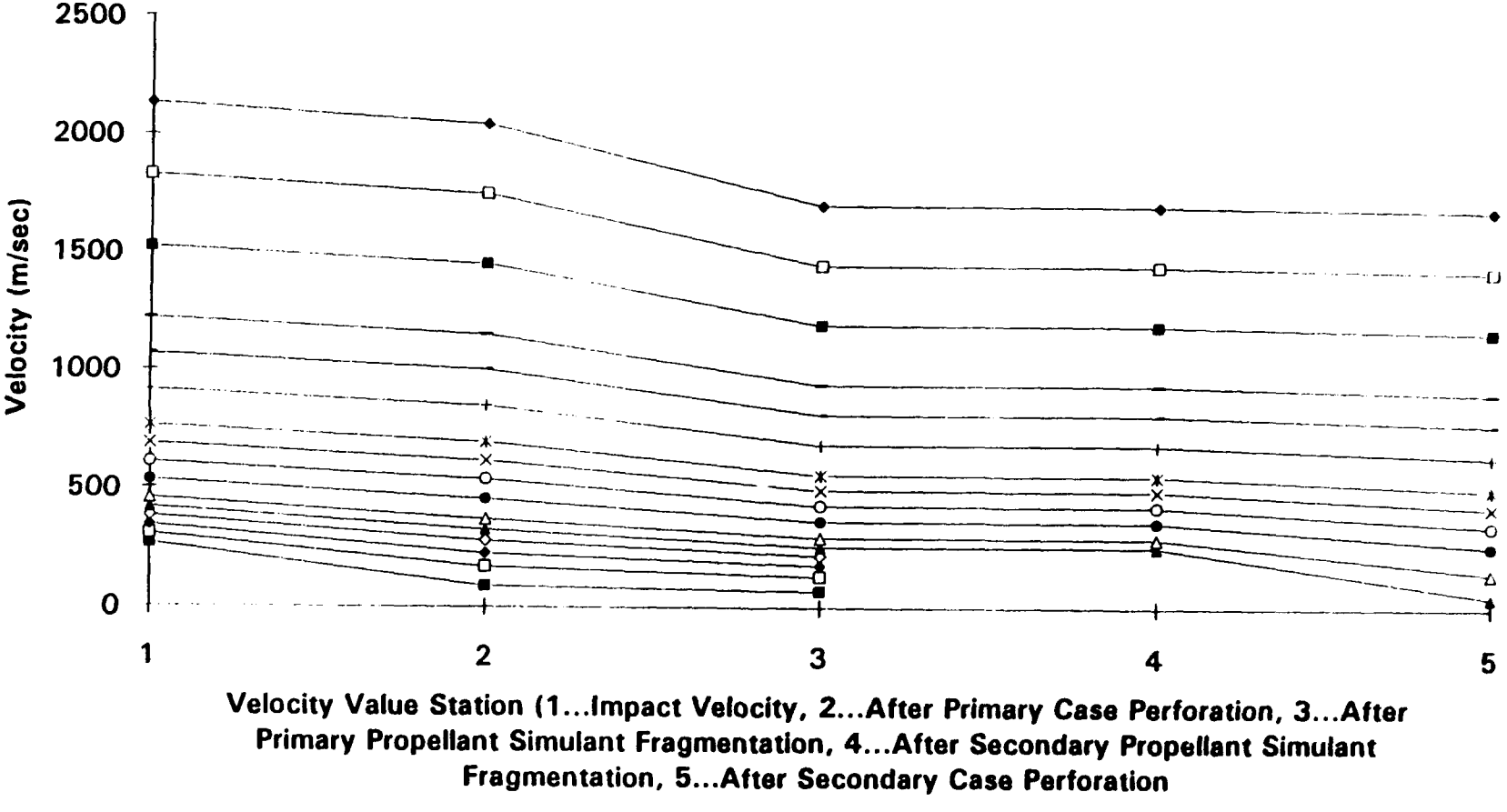

Figure 5. Projectile Velocity Decrease vs. Position Within Solid Rocket Motor

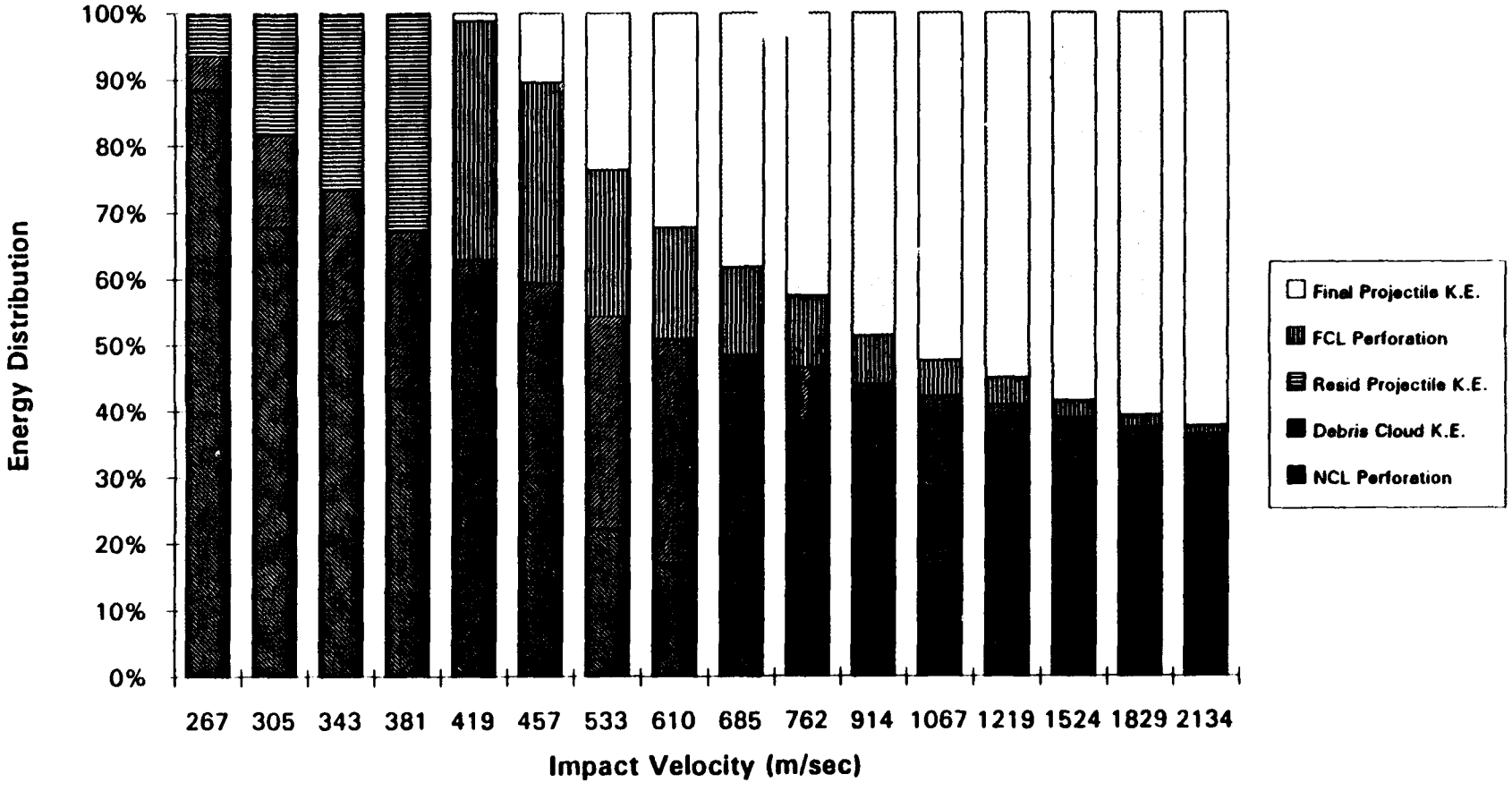

Figure 6. Partitioning of Initial Projectile Kinetic Energy
(NCL ... Near Case Layer, FCL ... Far Case Layer)

INITIAL DISTRIBUTION LIST

	No. of Copies
Dr. Charles E. Anderson, Jr. Southwest Research Institute P.O. Darwer 28510 San Antonio, Texas 78284	1
Mr. Charles Chase United Technologies Chemical Systems Division P.O. Box 49028 San Jose, California 95161-9028	1
Phillips Laboratory Dr. Robert Corley OLAC-RK/CA Edwards AFB, California 93523	3
Dr. Thomas L. Cost Mechanical & Aerospace Engineering Dept. University of Alabama in Huntsville Huntsville, Alabama 35899	1
Dr. Mark Director Director of Technology Atlantic Research Corporation 5945 Wellington Road Gainesville, Virgina 22065	1
Mr. Robert Grinsell Aeojet Propulsion Division P.O. Box 3222 Sacramento, California 95813-6000	1
Dr. Clark Hawk, Director Populsion Research Center University of Alabama in Huntsville Huntsville, Alabama 35899	1
Chemical Propulsion Information Agency Johns Hopkins University ATTN: H.L. Hoffman 10630 Little Patuxent Parkway Columbia, Maryland 21004-3200	1

Dr. Joseph Janni Chief Scientist Phillips Laboratory Kirtland AFB, NM 87117-6008	1
Dr. Gerald R.Karr, Interim Chair Civil Engineering Department University of Alabama in Huntsville Huntsville, Alabama 35899	1
Dr. Robert Keller Hercules Aerospace Corporation Bacchus Works, M/S B1 Magna, Utah 84044-0098	1
Dr. David Littlefield Southwest Research Institute P.O. Drawer 28510 San Antonio, Texas 78284	1
Commander U.S Naval Weapons Center ATTN: Code 3261, E. Lunstrom China Lake, California 93555-6001	1
Dr. Thomas A. Neely Research Institute University of Alabama in Huntsville Huntsville, Alabama 35899	1
Dr. Lynn D. Russell, Dean College of Engineering University of Alabama in Huntsville Huntsville, Alabama 35899	1
Dr. William P. Schonberg Civil Engineering Department University of Alabama in Huntsville Huntsville, Alabama 35899	5
Thiokol Incorporated ATTN: Bill Thomas P.O. Box 400006 Huntsville, Alabama 35899	1

Mr. Andy Victor Victor Technology 712 North Peg Street Ridgeway, California 93555	1
Mr. Cal Wiggens Thiokol Corporation 6767 Old Madison Pike Huntsville, Alabama 35806	1
U.S. Army Space and Strategic Defense Command P.O. Box 1500 ATTN: CSSD-TE-T Huntsville, Alabama 35807-3801	3
U.S. Army Space and Strategic Defense Command P.O. Box 1500 ATTN: CSSD-SL Huntsville, Alabama 35807-3801	1
U.S. Army Space and Strategic Defense Command P.O. Box 1500 ATTN: CSSD-IM-P Huntsville, Alabama 35807-3801	1
Dynamics Research Corporation SDIO Library, Suite 708 1755 Jefferson Davis Highway Crystal Square 5 Arlington, Virginia 22202	1
Defense Technical Information Center Cameron Station Alexandria, Virginia 22314	2
U.S. Army Missile Command ATTN: AMSMI-RD-ST-WF Mike Schexnayder Redstone Arsenal, Alabama 35898-5247	3
U.S. Army Missile Command ATTN: AMSMI-PD-PR-M Mr. Hodges Redstone Arsenal, Alabama 35898-5247	1

U.S. Army Missile Command
ATTN: AMSMI-PD-PR-M
Ms. Fisher
Redston Arsenal, Alabama 35898-5247 1

U.S. Army Missile Command
ATTN: AMSMI-PD-PR-M
Dr. Stephens
Redstone Arsenal, Alabama 35898-5247 1

U.S. Army Missile Command
ATTN: AMSMI-PD-PR
Dr. Ayers
Redstone Arsenal, Alabama 35898-5247 1